

Privacy-Preserving Data-Enabled Predictive Leading Cruise Control in Mixed Traffic

Kaixiang Zhang^{ID}, Kaian Chen^{ID}, Zhaojian Li^{ID}, *Senior Member, IEEE*,
 Jun Chen^{ID}, *Senior Member, IEEE*, and Yang Zheng^{ID}, *Member, IEEE*

Abstract—Data-driven predictive control of connected and automated vehicles (CAVs) has received increasing attention as it can achieve safe and optimal control without relying on explicit dynamical models. However, employing the data-driven strategy involves the collection and sharing of privacy-sensitive vehicle information, which is vulnerable to privacy leakage and might further lead to malicious activities. In this paper, we develop a privacy-preserving data-enabled predictive control scheme for CAVs in a mixed traffic environment, where human-driven vehicles (HDVs) and CAVs coexist. We tackle external eavesdroppers and honest-but-curious central unit eavesdroppers who wiretap the communication channel of the mixed traffic system and intend to infer the CAVs' state and input information. An affine masking-based privacy protection method is designed to conceal the true state and input signals, and an extended form of the data-enabled predictive leading cruise control under different data matrix structures is derived to achieve privacy-preserving optimal control for CAVs. Numerical simulations demonstrate that the proposed scheme can protect the privacy of CAVs against attackers without affecting control performance or incurring heavy computations.

Index Terms—Connected and automated vehicle, privacy preservation, data-driven control, mixed traffic.

I. INTRODUCTION

ADVANCES in wireless communication technologies such as vehicle-to-infrastructure (V2I) or vehicle-to-vehicle (V2V) offer modern vehicles with enhanced connectivity and new opportunities for intelligent and integrated vehicle control [1], [2]. One typical example is the cooperative adaptive cruise control (CACC), which regulates a convoy of vehicles to improve traffic flow stability, safety, and energy efficiency [3], [4], [5], [6]. While attracting much research interest, existing

Manuscript received 22 May 2022; revised 19 June 2023; accepted 16 October 2023. Date of publication 21 November 2023; date of current version 13 May 2024. This work was supported in part by the National Science Foundation (NSF) under Grant 2045436, Grant CMMI-2320698, and Grant CMMI-2320697. The work of Yang Zheng was supported in part by NSF under Grant ECCS-2154650. The Associate Editor for this article was A. Hajababae. (*Kaixiang Zhang and Kaian Chen contributed equally to this work.*) (*Corresponding author: Zhaojian Li.*)

Kaixiang Zhang, Kaian Chen, and Zhaojian Li are with the Department of Mechanical Engineering, Michigan State University, East Lansing, MI 48824 USA (e-mail: zhangk64@msu.edu; chenka@msu.edu; lizhaoj1@msu.edu).

Jun Chen is with the Department of Electrical and Computer Engineering, Oakland University, Rochester, MI 48309 USA (e-mail: junchen@oakland.edu).

Yang Zheng is with the Department of Electrical and Computer Engineering, University of California at San Diego, La Jolla, CA 92093 USA (e-mail: zhengy@ucsd.edu).

Digital Object Identifier 10.1109/TITS.2023.3329484

studies on CACC predominately focus on effective platooning of full connected and automated vehicles (CAVs). However, due to the gradual deployment of CAVs, it is expected that human-driven vehicles (HDVs) and CAVs will coexist for a long period of time, which raises the demand for developing cooperative control of CAVs in a mixed traffic flow.

HDVs often exhibit stochastic and uncertain behaviors that are difficult to characterize, making it challenging for the control design of CAVs in a mixed traffic environment. To address this issue, several approaches have been proposed. For instance, feedback controllers of CAVs are designed under the formation of connected cruise control in [7], [8], and [9], where CAVs can receive information from HDVs ahead. Leading cruise control (LCC) is proposed in [10], where CAVs make decisions by utilizing both the preceding and following HDVs' information. To handle the prediction uncertainty of HDVs, a robust platoon control framework is designed in [11] by leveraging tube model predictive control (MPC). We note that existing studies mainly focus on designing model-based approaches for CAVs [7], [8], [9], [10], [11], [12], [13]. One common strategy is to utilize car-following models to characterize the behavior of human drivers, e.g., optimal velocity model (OVM) [14] or intelligent driver model [15], enabling a state-space model of the mixed traffic system for system analysis and control design. Although model-based approaches can provide rigorous theoretical analysis and control synthesis when an accurate traffic model is available, it might not be applicable to real-world deployment since the parameters in human car-following models are non-trivial to identify accurately.

Instead of relying on explicit system models, data-driven approaches have recently emerged as an alternative to avoid model/parameter identification and directly incorporate collected data for control designs. For example, reinforcement learning (RL) [16], [17], [18] and adaptive dynamic programming (ADP) [19], [20], [21] have been developed to design optimal control schemes for CAVs. Although RL-based techniques can use experimental data to learn a model to simulate uncertain HDV behaviors, they are typically data intensive and have limited interpretability. On the other hand, data-driven ADP algorithms can provide optimal control actions, but they struggle to handle constraints that are critical to vehicle safety. Recent advances in data-driven MPC have shown promise to achieve optimal control with constraint and stability guarantees [22], [23]. In [24] and [25], a Data-EnablEd Predictive

Leading Cruise Control (DeeP-LCC) strategy is developed for a mixed traffic system, which can efficiently handle safety constraints among multiple CAVs and HDVs. Specifically, by leveraging the Data-EnabLeD Predictive Control (DeePC) techniques [26], input/output measurements are collected to first represent the mixed traffic system in a non-parametric manner, and to subsequently formulate a constrained optimization problem [24]. DeePC exploits behavioral system theory [27] and Willem's fundamental lemma [28] to implicitly describe the system trajectories without explicitly carrying out model identification. Its receding horizon implementation is shown to be equivalent to the MPC formulation for linear time-invariant (LTI) systems, and it has found various successes in several practical applications [29], [30].

Employing the DeeP-LCC approach for the control of CAVs in the mixed traffic, however, poses great concerns in privacy. To enable coordinated control, the onboard data of vehicles, which may contain private information, needs to be extensively collected and shared via wireless V2I or V2V communications, causing potential privacy leakage. Specifically, in a typical control architecture, each vehicle (both HDVs and CAVs) first sends its measured/estimated states to a central unit (e.g., a road-side edge or a remote cloud). The central unit then solves a pre-specified mixed-traffic optimal control problem and sends optimal control actions back to CAVs. In this setup, system measurements and control actions of CAVs need to be transmitted between the central unit and the local vehicles, raising concerns that an external eavesdropper or an honest-but-curious central unit can wiretap the communication channels to get sensitive information. In fact, several studies have shown that exposing local vehicle's information to connectivity can lead to security vulnerabilities and various malicious activities [31], [32], [33]. Failing to protect privacy can potentially lead to devastating effects for CAVs and other vehicles sharing the roadway.

The growing awareness of security in cyber-physical systems makes it imperative to protect privacy for CAV control in mixed traffic. So far, privacy and security problems have been studied under various intelligent vehicle scenarios [34], [35], [36]. In particular, numerous privacy-preserving approaches have been developed to enhance communication security of intelligent vehicles by leveraging conventional information technology privacy mechanisms, e.g., encryption [37], [38], secret sharing [39], and differential privacy [40], [41]. However, these approaches are not appropriate for the mixed traffic control considered in this work for two reasons. First, most of them are designed to protect the privacy of vehicles' information against the external eavesdropper, but cannot tackle honest-but-curious adversary which follows all communication/computation protocols correctly but is curious and uses received messages to infer vehicles' private information. Second, conventional privacy mechanisms either trade accuracy for privacy (e.g., differential privacy) or incur heavy computation/communication overhead (e.g., encryption), and hence are inappropriate for mixed traffic system subject to stringent accuracy and real-time constraints.

In this paper, we develop the first privacy-preserving data-enabled predictive control scheme for controlling CAVs in

mixed traffic. Specifically, we consider the same mixed traffic system in [24], where multiple CAVs and HDVs cooperate with each other under the LCC framework [10]. We show that if the central unit is an honest-but-curious adversary or there exists an external eavesdropper, the DeeP-LCC under both Hankel and Page matrix structures cannot protect the private information of the vehicles. To avoid leaking the state and input information of the CAVs, a simple yet effective affine masking-based privacy protection method is designed, which can mask the true state and input signals. After the affine masking, an extended DeeP-LCC is derived to generate safe and optimal control actions for the CAVs. We further introduce a privacy notion and show that the proposed affine masking-based method can protect the private system state and input signals from being inferred by the attackers. Some preliminary results are summarized in a conference version [42]. The new contributions of this work are as follows.

First, we study non-parametric representations of the mixed traffic system under both Hankel and Page matrix structures. The previous DeeP-LCC scheme [24] only leverages the Hankel matrix to store the collected data for non-parametric system representation. We extend DeeP-LCC with the Page matrix which is another effective structure for time-series data [43]. Second, we propose a privacy-preserving DeeP-LCC method for mixed traffic control, which can retain the advantages of the original DeeP-LCC while avoiding privacy leakage. Specifically, we conceal the privacy-sensitive state and input signals of CAVs via affine masking and reformulate a compatible DeeP-LCC that is equivalent to the original one. Although affine masking has been utilized for privacy protection in cloud-based MPC [44], [45], its application in data-driven approaches has not been thoroughly explored. The challenge arises from the fundamental differences between data-driven control and MPC in problem formulation and theoretical analysis. In this paper, we successfully incorporate affine masking with data-driven predictive control to enhance the privacy protection of the mixed traffic system. This newly developed DeeP-LCC is a non-trivial extension that ends with a new DeePC structure and provable privacy guarantees. The affine masking-based method is light-weight in computation, making it suitable for CAV controls that have fast dynamics. Finally, we conduct extensive traffic simulations to validate the performance of the privacy-preserving DeeP-LCC. The results demonstrate the benefits of our proposed method in terms of not only improving traffic smoothness and fuel economy, but also protecting privacy against potential attackers.

The remainder of this paper is organized as follows. Section II introduces background notations and formulates the mixed traffic control problem. Section III provides an overview of DeeP-LCC method from [24]. Section IV presents the affine masking-based privacy protection method and the extended DeeP-LCC. Section V analyses the equivalence and privacy-preserving properties of the developed method. Simulations are shown in Section VI. Finally, we conclude the paper in Section VII.

Notations: We denote \mathbb{R} and \mathbb{Z}_+ as the set of real numbers and positive integers, respectively. 0_n and $0_{n \times m}$ are denoted as a zero vector of size n and a zero matrix of size $n \times m$,

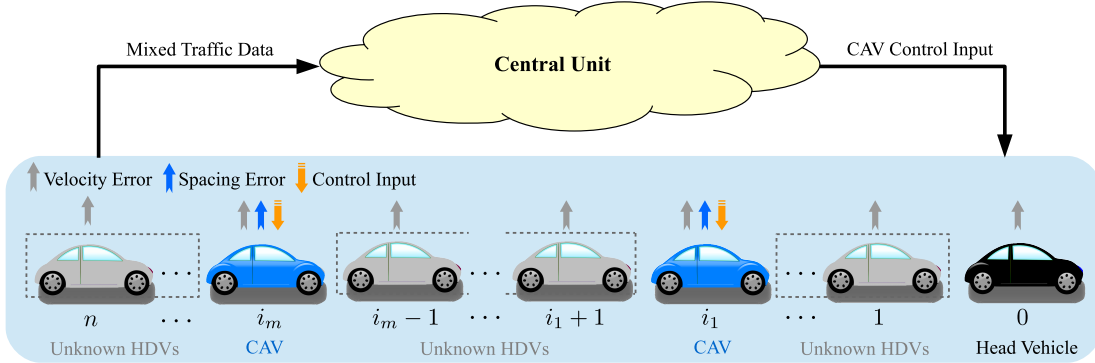


Fig. 1. Schematic of mixed traffic system with $n+1$ vehicles.

respectively. 1_n and I_n are denoted as an $n \times 1$ vector with all entries being ones and an $n \times n$ identity matrix, respectively. Denote $\text{diag}(a_1, \dots, a_n)$ as a diagonal matrix with a_1, \dots, a_n on its diagonal entries, and $\text{diag}(A_1, \dots, A_n)$ as a block-diagonal matrix with matrices A_1, \dots, A_n on its diagonal blocks. e_n^m is used to denote an $n \times 1$ vector, with the m -th entry being one and the others being zero.

II. MODELING AND PROBLEM STATEMENT

A. System Model of Mixed Traffic

As shown in Fig. 1, we consider a mixed traffic system consisting of $n+1$ vehicles: one head vehicle (indexed as 0), m CAVs, and $n-m$ HDVs. The head vehicle is controlled by a human driver. Let $\Omega = \{1, 2, \dots, n\}$ be the set of vehicle indices ordered from front to end. The sets of CAV indices and HDV indices are denoted by $\Omega_C = \{i_1, i_2, \dots, i_m\} \subseteq \Omega$ and $\Omega_H = \{j_1, j_2, \dots, j_{n-m}\} = \Omega \setminus \Omega_C$, respectively, where $i_1 < i_2 < \dots < i_m$ and $j_1 < j_2 < \dots < j_{n-m}$. We use $p_i(t)$, $v_i(t)$ and $a_i(t)$ to denote the position, velocity and acceleration of the i -th vehicle at time t , respectively.

The car-following dynamics for HDVs are modeled by the following nonlinear processes:

$$\dot{v}_i(t) = F(s_i(t), \dot{s}_i(t), v_i(t)), \quad i \in \Omega_H, \quad (1)$$

where $s_i(t) = p_{i-1}(t) - p_i(t)$ and $\dot{s}_i(t) = v_{i-1}(t) - v_i(t)$ are the relative spacing and velocity between vehicle i and its preceding vehicle $i-1$, respectively. Denote s^* and v^* as the equilibrium spacing and equilibrium velocity of the mixed traffic system. Then the spacing error and velocity error of vehicle i are defined as $\tilde{s}_i(t) = s_i(t) - s^*$ and $\tilde{v}_i(t) = v_i(t) - v^*$, respectively. By applying the first-order Taylor expansion on (1) at the equilibrium (s^*, v^*) , the linearized model for each HDV can be obtained

$$\begin{cases} \dot{\tilde{s}}_i(t) = \tilde{v}_{i-1}(t) - \tilde{v}_i(t), \\ \dot{\tilde{v}}_i(t) = \alpha_1 \tilde{s}_i(t) - \alpha_2 \tilde{v}_i(t) + \alpha_3 \tilde{v}_{i-1}(t), \end{cases} \quad i \in \Omega_H, \quad (2)$$

with $\alpha_1 = \frac{\partial F}{\partial s}, \alpha_2 = \frac{\partial F}{\partial \dot{s}} - \frac{\partial F}{\partial v}, \alpha_3 = \frac{\partial F}{\partial \ddot{s}}$ evaluated at the equilibrium state (s^*, v^*) . In this paper, we use the OVM [14] model to describe the HDVs' car-following dynamics in (1). More details about the linearized model of OVM model can be found in [12] and [13]. For the CAV, the acceleration is

used as the control input, i.e., $\dot{v}_i(t) = u_i(t)$, $i \in \Omega_C$, and its system model is described by

$$\begin{cases} \dot{\tilde{s}}_i(t) = \tilde{v}_{i-1}(t) - \tilde{v}_i(t), \\ \dot{\tilde{v}}_i(t) = u_i(t), \end{cases} \quad i \in \Omega_C. \quad (3)$$

The state of each vehicle is denoted by $x_i(t) = [\tilde{s}_i, \tilde{v}_i]^\top$, and the overall state of the mixed traffic system is defined as

$$x(t) = [x_1^\top(t), x_2^\top(t), \dots, x_n^\top(t)]^\top \in \mathbb{R}^{2n}.$$

Based on (2) and (3), the linearized state-space model for the mixed traffic system can be derived, as follows:

$$\dot{x}(t) = Ax(t) + Bu(t) + H\epsilon(t), \quad (4)$$

where $u(t) = [u_{i_1}(t), u_{i_2}(t), \dots, u_{i_m}(t)]^\top$ is the collective control input and $\epsilon(t) = \tilde{v}_0(t) = v_0(t) - v^*$ is the velocity error of the head vehicle. The system matrices in (4) are

$$A = \begin{bmatrix} A_{1,1} & & & \\ A_{2,2} & A_{2,1} & & \\ & \ddots & \ddots & \\ & & A_{n-1,2} & A_{n-1,1} \\ & & & A_{n,2} & A_{n,1} \end{bmatrix} \in \mathbb{R}^{2n \times 2n},$$

$$B = [e_{2n}^{2i_1}, e_{2n}^{2i_2}, \dots, e_{2n}^{2i_m}] \in \mathbb{R}^{2n \times m},$$

$$H = [1, \alpha_3, 0_{2n-2}^\top]^\top \in \mathbb{R}^{2n},$$

where

$$\begin{cases} A_{i,1} = \begin{bmatrix} 0 & -1 \\ \alpha_1 & -\alpha_2 \end{bmatrix}, \quad A_{i,2} = \begin{bmatrix} 0 & 1 \\ 0 & \alpha_3 \end{bmatrix}, \quad i \in \Omega_H; \\ A_{i,1} = \begin{bmatrix} 0 & -1 \\ 0 & 0 \end{bmatrix}, \quad A_{i,2} = \begin{bmatrix} 0 & 1 \\ 0 & 0 \end{bmatrix}, \quad i \in \Omega_C. \end{cases}$$

Recent works on mixed traffic control [8], [10], [12], [13], [19], [20], [21] require that both the spacing error and velocity error of HDVs are available. However, as discussed in [24], the spacing error of HDVs (i.e., \tilde{s}_i ($i \in \Omega_H$)) is impractical to be observed due to the unknown human driving behavior. Therefore, the output signal of the mixed traffic system is constructed as

$$y(t) = [x_{i_1}^\top(t), \dots, x_{i_m}^\top(t), \tilde{v}_{j_1}(t), \dots, \tilde{v}_{j_{n-m}}(t)]^\top,$$

where $y(t) \in \mathbb{R}^{n+m}$ consists of all state measurements of the CAVs, i.e., \tilde{s}_i, \tilde{v}_i ($i \in \Omega_C$), and the velocity error signal of the HDVs, i.e., \tilde{v}_i ($i \in \Omega_H$). The output $y(t)$ can be related to the overall state $x(t)$ via

$$y(t) = Cx(t), \quad (5)$$

with

$$C = \left[e_{2n}^{2i_1-1}, e_{2n}^{2i_1}, \dots, e_{2n}^{2i_m-1}, e_{2n}^{2i_m}, e_{2n}^{2j_1}, e_{2n}^{2j_2}, \dots, e_{2n}^{2j_{n-m}} \right]^\top$$

being the output matrix. Given the sampling interval $\Delta t > 0$, the continuous-time model in (4) and (5) can be transformed into the discrete-time

$$\begin{cases} x(k+1) = A_d x(k) + B_d u(k) + H_d \epsilon(k), \\ y(k) = C_d x(k), \end{cases} \quad (6)$$

where $A_d = e^{A\Delta t} \in \mathbb{R}^{2n \times 2n}$, $B_d = \int_0^{\Delta t} e^{At} B dt \in \mathbb{R}^{2n \times m}$, $H_d = \int_0^{\Delta t} e^{At} H dt \in \mathbb{R}^{2n}$, $C_d = C \in \mathbb{R}^{(n+m) \times 2n}$. Let $\hat{u}(k) = [\epsilon(k), u^\top(k)]^\top$ be the combined inputs signal and $\hat{B}_d = [H_d, B_d]$ be the combined input matrix. Then (6) can be rewritten into a compact form as follows:

$$\begin{cases} x(k+1) = A_d x(k) + \hat{B}_d \hat{u}(k), \\ y(k) = C_d x(k). \end{cases} \quad (7)$$

In this paper, we assume that $\alpha_1 - \alpha_2 \alpha_3 + \alpha_3^2 \neq 0$ in (2), which ensures that the mixed traffic system is stabilizable and observable [10]. Note that the above model is only used for analysis, and the controller design in Section III does not assume the exact model (6).

B. Problem Statement

As shown in Fig. 1, the mixed traffic system utilizes a central unit (e.g., a road-side edge or a remote cloud) to receive all vehicle data and generate the control signals for CAVs. Specifically, each CAV needs to send its state $x_i(k) = [\tilde{s}_i(k), \tilde{v}_i(k)]^\top$ ($i \in \Omega_C$) to the central unit, while the head vehicle and HDVs are requested to provide the velocity error $\epsilon(k)$ and $\tilde{v}_i(k)$ ($i \in \Omega_H$), respectively. Then, the central unit solves a pre-specified control problem and sends control inputs $u_i(k)$ ($i \in \Omega_C$) to the CAVs.

For mixed traffic control, one challenge lies in the unknown HDVs' car-following dynamics, which are difficult to identify due to stochastic and uncertain human behaviors. In addition, the mixed traffic system requires extensive data transmission between vehicles and central unit, which raises concerns of privacy leakage. Therefore, the main objective of this paper is to design a privacy-preserving data-driven control scheme, which can improve the traffic efficiency of the vehicle fleet without relying on an explicit system model and protect private vehicles' information against attackers. The design details are presented in Sections III and IV.

III. DATA-ENABLED PREDICTIVE LEADING CRUISE CONTROL

In this section, we first discuss the non-parametric representations of the mixed traffic system based on Hankel and Page matrix structures and then briefly review the DeeP-LCC scheme from [24].

A. Non-Parametric Representation of Mixed Traffic

Conventional methods rely on explicit system model (6) to facilitate controller design. One typical example is MPC whose performance depends closely on the model accuracy. Even though there exist many system identification techniques, it is still difficult to obtain accurate models for complex systems such as the mixed traffic system with stochastic and uncertain human driving behavior. The DeePC [26] is a promising model-free paradigm and recently has been leveraged by [24] to design the DeeP-LCC scheme for mixed traffic. In particular, based on Willems' fundamental lemma [28], this class of data-driven approaches can describe the dynamical system in a non-parametric manner.

Both Hankel matrix and Page matrix can be utilized to facilitate the non-parametric representation of dynamic systems. Given a signal $\omega \in \mathbb{R}^q$ and two integers $i, j \in \mathbb{Z}_+$ with $i \leq j$, we denote by $\omega_{[i,j]}$ the restriction of ω to the interval $[i, j]$, namely, $\omega_{[i,j]} := [\omega^\top(i), \omega^\top(i+1), \dots, \omega^\top(j)]^\top$. To simplify notation, we will also use $\omega_{[i,j]}$ to denote the sequence $\{\omega(i), \dots, \omega(j)\}$. The Hankel matrix of depth k associated with $\omega_{[i,j]}$ is defined as

$$\mathcal{H}_k(\omega_{[i,j]}) := \begin{bmatrix} \omega(i) & \omega(i+1) & \dots & \omega(j-k+1) \\ \omega(i+1) & \omega(i+2) & \dots & \omega(j-k+2) \\ \vdots & \vdots & \ddots & \vdots \\ \omega(i+k-1) & \omega(i+k) & \dots & \omega(j) \end{bmatrix}$$

Meanwhile, the Page matrix of depth k associated with $\omega_{[i,j]}$ is defined as

$$\mathcal{P}_k(\omega_{[i,j]}) := \begin{bmatrix} \omega(i) & \omega(i+k) & \dots & \omega(i+\lfloor \frac{j-i+1}{k} \rfloor k) \\ \omega(i+1) & \omega(i+k+1) & \dots & \omega(i+\lfloor \frac{j-i+1}{k} \rfloor k+1) \\ \vdots & \vdots & \ddots & \vdots \\ \omega(i+k-1) & \omega(i+2k-1) & \dots & \omega(i+\lfloor \frac{j-i+1}{k} \rfloor k-1) \end{bmatrix},$$

where $\lfloor \cdot \rfloor$ is the floor function which rounds its argument down to the nearest integer.

Definition 1 ([23]): The sequence $\omega_{[i,j]}$ is said to be

- Hankel exciting of order k if the matrix $\mathcal{H}_k(\omega_{[i,j]})$ has full row rank;
- k -Page exciting of order l , where $l \in \mathbb{Z}_+$, if the matrix

$$\begin{bmatrix} \mathcal{P}_k(\omega_{[i,j-(l-1)k]}) \\ \mathcal{P}_k(\omega_{[k+i,j-(l-2)k]}) \\ \vdots \\ \mathcal{P}_k(\omega_{[k(l-1)+i,j]}) \end{bmatrix}$$

has full row rank.

We now discuss the non-parametric representation of mixed traffic system (6). It begins with data collection. Specifically, a trajectory of length $T \in \mathbb{Z}_+$ is collected from the mixed traffic system (6), which includes the following two parts:

- a combined input sequence of the mixed traffic system

$$\hat{u}_{[1,T]}^d = \begin{bmatrix} \hat{u}^d(1) \\ \vdots \\ \hat{u}^d(T) \end{bmatrix} \in \mathbb{R}^{(m+1)T},$$

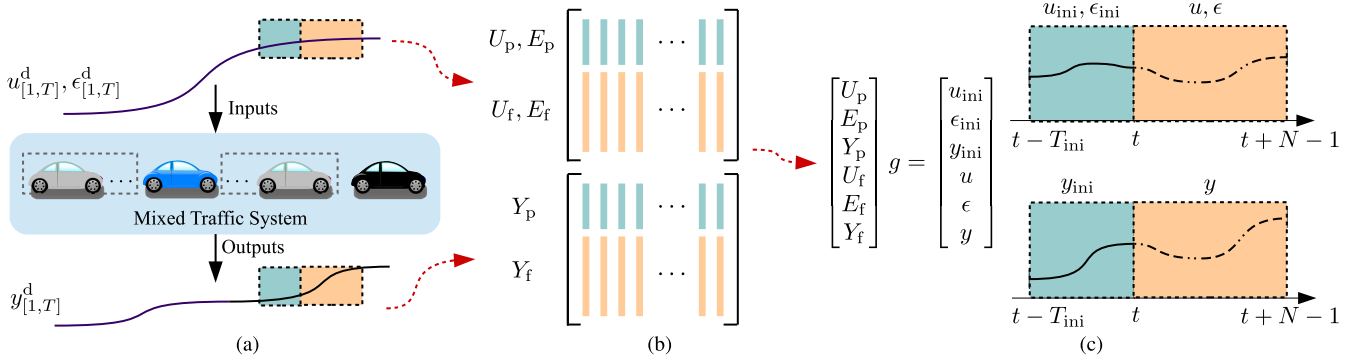


Fig. 2. Interpretation of Propositions 1 and 2. (a) A consecutive length-\$T\$ input/output trajectory is collected from the mixed traffic system. (b) All consecutive length-\$(T_{\text{ini}} + N)\$ trajectories are extracted to construct the Hankel matrix (Proposition 1) or the Page matrix (Proposition 2). In particular, each trajectory is divided into two parts, i.e., ‘previous data’ of length \$T_{\text{ini}}\$ colored in cyan and ‘future data’ of length \$N\$ colored in orange. (c) All valid length-\$(T_{\text{ini}} + N)\$ trajectories of the mixed traffic system can be captured by the Hankel matrix or Page matrix.

which is comprised of CAVs’ acceleration sequence and the velocity error sequence of the head vehicle, i.e.,

$$u_{[1,T]}^d = \begin{bmatrix} u^d(1) \\ \vdots \\ u^d(T) \end{bmatrix} \in \mathbb{R}^{mT}, \epsilon_{[1,T]}^d = \begin{bmatrix} \epsilon^d(1) \\ \vdots \\ \epsilon^d(T) \end{bmatrix} \in \mathbb{R}^T;$$

- the corresponding output sequence

$$y_{[1,T]}^d = \begin{bmatrix} y^d(1) \\ \vdots \\ y^d(T) \end{bmatrix} \in \mathbb{R}^{(n+m)T}.$$

After collecting these data sequences, different matrix structures can be used to store them for non-parametric representation. The Hankel matrix is the commonly used one [24], [26]. Specifically, under the Hankel matrix structure, the data sequences are divided into two parts, i.e., the ‘previous data’ of length \$T_{\text{ini}} \in \mathbb{Z}_+\$ and ‘future data’ of length \$N \in \mathbb{Z}_+\$, to construct the following matrices:

$$\begin{aligned} \begin{bmatrix} U_p^{\mathcal{H}} \\ U_f^{\mathcal{H}} \end{bmatrix} &:= \mathcal{H}_{T_{\text{ini}}+N}(u_{[1,T]}^d), \quad \begin{bmatrix} E_p^{\mathcal{H}} \\ E_f^{\mathcal{H}} \end{bmatrix} := \mathcal{H}_{T_{\text{ini}}+N}(\epsilon_{[1,T]}^d), \\ \begin{bmatrix} Y_p^{\mathcal{H}} \\ Y_f^{\mathcal{H}} \end{bmatrix} &:= \mathcal{H}_{T_{\text{ini}}+N}(y_{[1,T]}^d), \end{aligned} \quad (8)$$

where \$U_p^{\mathcal{H}}\$ denotes the first \$T_{\text{ini}}\$ block rows of \$\mathcal{H}_{T_{\text{ini}}+N}(u_{[1,T]}^d)\$ and \$U_f^{\mathcal{H}}\$ denotes the last \$N\$ block rows of \$\mathcal{H}_{T_{\text{ini}}+N}(u_{[1,T]}^d)\$, respectively (similarly for \$E_p^{\mathcal{H}}, E_f^{\mathcal{H}}\$ and \$Y_p^{\mathcal{H}}, Y_f^{\mathcal{H}}\$).

Let \$u_{\text{ini}} = u_{[t-T_{\text{ini}}, t-1]}\$ be the control input sequence within a past time horizon of length \$T_{\text{ini}}\$, and \$u = u_{[t, t+N-1]}\$ be the control input sequence within a prediction horizon of length \$N\$ (similarly for \$\epsilon_{\text{ini}}, \epsilon\$ and \$y_{\text{ini}}, y\$). Based on Willems’ fundamental lemma [28] and the DeePC [26], we have the following proposition.

Proposition 1: Consider a controllable mixed traffic system (6) and assume that the combined input sequence \$\hat{u}_{[1,T]}^d\$ is Hankel exciting of order \$T_{\text{ini}} + N + 2n\$. Then, any trajectory \$(u_{\text{ini}}, \epsilon_{\text{ini}}, y_{\text{ini}}, u, \epsilon, y)\$ of the mixed traffic system (6) can be

constructed via

$$\begin{bmatrix} U_p^{\mathcal{H}} \\ E_p^{\mathcal{H}} \\ Y_p^{\mathcal{H}} \\ U_f^{\mathcal{H}} \\ E_f^{\mathcal{H}} \\ Y_f^{\mathcal{H}} \end{bmatrix} g = \begin{bmatrix} u_{\text{ini}} \\ \epsilon_{\text{ini}} \\ y_{\text{ini}} \\ u \\ \epsilon \\ y \end{bmatrix}, \quad (9)$$

where \$g \in \mathbb{R}^{T-T_{\text{ini}}-N+1}\$.

Previous work [24] relies on arranging the data sequences into Hankel matrices for non-parametric representation of the mixed traffic system. Here, we also explore another effective structure, i.e., the Page matrix structure, to arrange the data sequences. Similar to (8), the data sequences are partitioned into two parts using Page matrices, as follows:

$$\begin{aligned} \begin{bmatrix} U_p^{\mathcal{P}} \\ U_f^{\mathcal{P}} \end{bmatrix} &:= \mathcal{P}_{T_{\text{ini}}+N}(u_{[1,T]}^d), \quad \begin{bmatrix} E_p^{\mathcal{P}} \\ E_f^{\mathcal{P}} \end{bmatrix} := \mathcal{P}_{T_{\text{ini}}+N}(\epsilon_{[1,T]}^d), \\ \begin{bmatrix} Y_p^{\mathcal{P}} \\ Y_f^{\mathcal{P}} \end{bmatrix} &:= \mathcal{P}_{T_{\text{ini}}+N}(y_{[1,T]}^d), \end{aligned} \quad (10)$$

where \$U_p^{\mathcal{P}}\$ denotes the first \$T_{\text{ini}}\$ block rows of \$\mathcal{P}_{T_{\text{ini}}+N}(u_{[1,T]}^d)\$ and \$U_f^{\mathcal{P}}\$ denotes the last \$N\$ block rows of \$\mathcal{P}_{T_{\text{ini}}+N}(u_{[1,T]}^d)\$, respectively (similarly for \$E_p^{\mathcal{P}}, E_f^{\mathcal{P}}\$ and \$Y_p^{\mathcal{P}}, Y_f^{\mathcal{P}}\$). Based on Theorem 2.1 in [23], the non-parametric representation of the mixed traffic system can be formulated with the Page matrix structure as follows:

Proposition 2: Consider a controllable mixed traffic system (6) and assume that the combined input sequence \$\hat{u}_{[1,T]}^d\$ is \$(T_{\text{ini}} + N)\$-Page exciting of order \$2n + 1\$. Then, any trajectory \$(u_{\text{ini}}, \epsilon_{\text{ini}}, y_{\text{ini}}, u, \epsilon, y)\$ of the mixed traffic system (6) can be constructed via

$$\begin{bmatrix} U_p^{\mathcal{P}} \\ E_p^{\mathcal{P}} \\ Y_p^{\mathcal{P}} \\ U_f^{\mathcal{P}} \\ E_f^{\mathcal{P}} \\ Y_f^{\mathcal{P}} \end{bmatrix} g = \begin{bmatrix} u_{\text{ini}} \\ \epsilon_{\text{ini}} \\ y_{\text{ini}} \\ u \\ \epsilon \\ y \end{bmatrix}, \quad (11)$$

where \$g \in \mathbb{R}^{\lfloor \frac{T}{T_{\text{ini}}+N} \rfloor}\$.

Fig. 2 shows a schematic of Propositions 1 and 2. Propositions 1 and 2 reveal that by collecting sufficiently rich traffic data, one can directly predict the valid trajectories of the mixed traffic system without requiring an explicit model of HDVs.

Remark 1: To satisfy the Hankel excitation condition in Proposition 1, one should collect a minimum of $(m+2)(T_{\text{ini}} + N + 2n) - 1$ data samples, i.e., $T \geq (m+2)(T_{\text{ini}} + N + 2n) - 1$; on the other hand, to satisfy the Page excitation condition in Proposition 2, one requires that $T \geq (T_{\text{ini}} + N)((m+1)(T_{\text{ini}} + N) + 1)(2n + 1) - 1$. \square

Remark 2: The main difference between the Hankel matrix and the Page matrix is that none of the entries in the latter are repeated. This has both advantages and disadvantages. The main disadvantage is that more data samples are needed to construct the matrix, and thus the data collection is more expensive. However, more data samples usually contain more system information, which is conducive to achieving non-parametric system representation. In addition, if the measurements are corrupted by noise, the entries of the Page matrix are statistically independent, leading to algorithmically favourable properties, e.g., singular value decomposition can be used for de-noising [29]. \square

B. DeeP-LCC Formulation

Propositions 1 and 2 reveal that if sufficiently rich traffic data is collected, the future trajectory of the mixed traffic system can be directly predicted without relying on explicit system model. The relations (9) and (11) are the non-parametric representations of the mixed traffic system, which are the key in formulating the DeeP-LCC.

More precisely, at each time step t , the control actions of the CAVs are generated by solving the following optimization problem:

$$\begin{aligned} & \min_{g, u, y} J(y, u) = \sum_{k=t}^{t+N-1} \left(\|y(k)\|_Q^2 + \|u(k)\|_R^2 \right) \\ & \text{s.t. } (9) \text{ (or (11)),} \\ & \quad \epsilon = 0_N, \\ & \quad y_{\min} \leq y(k) \leq y_{\max}, \quad k = t, \dots, t + N - 1, \\ & \quad a_{\min} \leq u(k) \leq a_{\max}, \quad k = t, \dots, t + N - 1. \end{aligned} \quad (12)$$

In (12), $J(y, u)$ is a quadratic cost function, and its weighting matrices Q and R are selected as $Q = \text{diag}(Q_C, Q_H) \in \mathbb{R}^{(n+m) \times (n+m)}$ with $Q_C = \text{diag}(w_s, w_v, \dots, w_s, w_v) \in \mathbb{R}^{2m \times 2m}$, $Q_H = \text{diag}(w_v, \dots, w_v) \in \mathbb{R}^{(n-m) \times (n-m)}$ and $R = \text{diag}(w_u, \dots, w_u) \in \mathbb{R}^{m \times m}$, where w_s , w_v , w_u are the weighting factors for the spacing error of CAVs, the velocity error of all vehicles, and the control input of CAVs, respectively. The second constraint, $\epsilon = 0_N$, is used to predict the future velocity error sequence of the head vehicle. The third constraint is applied to the output of the mixed traffic system for safety guarantees, and the lower and upper bounds of the output signal are defined as

$$\begin{aligned} y_{\min} &= \left[(1_m \otimes [\tilde{s}_{\min}, \tilde{v}_{\min}]^\top)^\top, (1_{n-m} \otimes \tilde{v}_{\min})^\top \right]^\top \\ y_{\max} &= \left[(1_m \otimes [\tilde{s}_{\max}, \tilde{v}_{\max}]^\top)^\top, (1_{n-m} \otimes \tilde{v}_{\max})^\top \right]^\top \end{aligned}$$

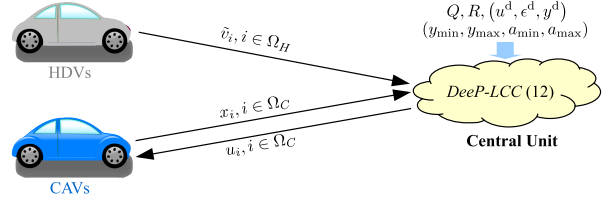


Fig. 3. Unsecure DeeP-LCC architecture.

with $\tilde{s}_{\min}, \tilde{s}_{\max}$ ($\tilde{v}_{\min}, \tilde{v}_{\max}$) being the lower and upper bounds of spacing (velocity) error. The fourth constraint in (12) is applied to the input of the mixed traffic system, and a_{\min}, a_{\max} denote the lower and upper bounds of input signal. We refer the interested reader to [24] for more details on designing the cost function and constraints in DeeP-LCC.

IV. PRIVACY-PRESERVING DEEP-LCC

In this section, we first introduce the attack models and then present an affine masking strategy. We finally propose a new privacy-preserving DeeP-LCC.

A. Attack Models

For the mixed-traffic vehicle fleet discussed above, a central unit (e.g., a road-side edge compute or a remote cloud) is needed to receive all the vehicle data and solve the optimization problem (12). A feasible architecture is shown in Fig. 3 and is described as follows:

- *Handshaking Phase:* The vehicle system sends

$$\left\{ Q, R, (u_{[1,T]}^d, \epsilon_{[1,T]}^d, y_{[1,T]}^d), (y_{\min}, y_{\max}, a_{\min}, a_{\max}) \right\}$$

to the central unit, which are the necessary information for the central unit to set up the optimization problem (12).

- *Execution Phase:* At each time step k , each CAV and HDV sends its state $x_i(k) = [\tilde{s}_i(k), \tilde{v}_i(k)]^\top$ ($i \in \Omega_C$) and velocity error $\tilde{v}_i(k)$ ($i \in \Omega_H$), respectively, to the central unit. The central unit computes $u(k)$ by solving the optimization problem (12) and sends optimal $u_i(k)$ ($i \in \Omega_C$) to the CAVs. Finally, the CAVs applies $u_i(k)$ to the actuators and the system evolves over one step.

The involved vehicles need to provide the central unit with real-time measurements, pre-collected data, cost function, and constraints to facilitate the calculation of (12). The data may contain private contents that need to be protected from external attackers. In this paper, we consider two attack models [36]:

- *Eavesdropping attacks* are attacks in which an external eavesdropper wiretaps communication channels to intercept exchanged messages in an attempt to learn the information about sending parties.
- *Honest-but-curious attacks* are attacks in which the untrusted central unit follows the protocol steps correctly but is curious and collects received intermediate data in an attempt to learn the information about the vehicles.

In particular, we consider the case that the privacy-sensitive information is contained in the system state and input of CAVs,

i.e., $x_i(k) = [\tilde{s}_i(k), \tilde{v}_i(k)]^\top$, $u_i(k)$, $i \in \Omega_C$. It is apparent that the attacker can successfully eavesdrop the messages $x_i(k)$ and $u_i(k)$ when the DeeP-LCC architecture introduced in Section III-B is adopted.

In the next subsection, we develop a masking mechanism to modify the exchanged information between the CAVs and the central unit such that an equivalent data-enabled predictive control problem is solved without affecting system performance while preventing the attacker from wiretapping the CAVs' state and input. Although we only consider the privacy preservation for CAVs, the following proposed approach can also be straightforwardly adopted by HDVs to mask privacy-sensitive information, e.g., velocity error $\tilde{v}_i(k)$, $i \in \Omega_H$.

B. Affine Masking

Affine masking is a class of algebraic transformations and recently has been adopted to accomplish privacy protection for cloud-based control [44], [45]. In this paper, by considering the characteristics of the mixed traffic system, we introduce affine transformation maps to design a privacy-preserved DeeP-LCC scheme. Specifically, for each CAV, two invertible affine maps are employed to transform the state $x_i(k)$ and input $u_i(k)$ to the new state $\bar{x}_i(k)$ and input $\bar{u}_i(k)$, as follows:

$$\begin{cases} \bar{x}_i(k) = P_{x,i}x_i(k) + l_{x,i}, \\ \bar{u}_i(k) = P_{u,i}u_i(k) + l_{u,i}, \end{cases} \quad \forall i \in \Omega_C, \quad (13)$$

where $P_{x,i} \in \mathbb{R}^{2 \times 2}$ is an arbitrary invertible matrix, and $l_{x,i} \in \mathbb{R}^2$, $P_{u,i} \in \mathbb{R}$ and $l_{u,i} \in \mathbb{R}$ are arbitrary non-zero vector or constant with compatible dimensions. After each CAV masks its true state and input via (13), the new input and output signals of the mixed traffic system are defined as

$$\begin{aligned} \bar{u}(k) &= [\bar{u}_{i_1}(k), \bar{u}_{i_2}(k), \dots, \bar{u}_{i_m}(k)]^\top, \\ \bar{y}(k) &= [\bar{x}_{i_1}^\top(k), \dots, \bar{x}_{i_m}^\top(k), \tilde{v}_{j_1}(k), \dots, \tilde{v}_{j_{n-m}}(k)]^\top. \end{aligned} \quad (14)$$

Based on (13), (14) and the definition of $u(k)$ and $y(k)$, we obtain that

$$\bar{u}(k) = P_u u(k) + L_u, \quad \bar{y}(k) = P_y y(k) + L_y, \quad (15)$$

where

$$\begin{aligned} P_u &= \text{diag}(P_{u,i_1}, P_{u,i_2}, \dots, P_{u,i_m}) \in \mathbb{R}^{m \times m}, \\ L_u &= [l_{u,i_1}, l_{u,i_2}, \dots, l_{u,i_m}]^\top \in \mathbb{R}^m, \\ P_y &= \text{diag}(P_{x,i_1}, \dots, P_{x,i_m}, I_{n-m}) \in \mathbb{R}^{(n+m) \times (n+m)}, \\ L_y &= [l_{x,i_1}^\top, \dots, l_{x,i_m}^\top, 0_{n-m}^\top]^\top \in \mathbb{R}^{(n+m)}. \end{aligned}$$

In (15), (P_u, L_u) and (P_y, L_y) are two affine maps constructed from the local affine maps of CAVs, and are used to transform the original input and output of mixed traffic system, i.e., $(u(k), y(k))$, into the new ones $(\bar{u}(k), \bar{y}(k))$. Given the affine transformation, the discrete-time model of the mixed traffic system (6) can be reformulated as follows:

$$\begin{cases} x(k+1) = A_d x(k) + \bar{B}_d \bar{u}(k) + H_d \epsilon(k) + \bar{L}_u, \\ \bar{y}(k) = \bar{C}_d x(k) + L_y, \end{cases} \quad (16)$$

where $\bar{B}_d = B_d P_u^{-1}$, $\bar{L}_u = -B_d P_u^{-1} L_u$, and $\bar{C}_d = P_y C_d$.

Under the affine transformation mechanism (14), the exchanged information between the CAVs and the central unit changes to $\bar{x}_i(k)$, $\bar{u}_i(k)$, $i \in \Omega_C$, which can avoid leaking the real state and input signals to the eavesdropper or the central unit. This affine transformation mechanism also leads to a new system formulation (16), and thus a compatible DeeP-LCC method needs to be developed.

C. Privacy-Preserving DeeP-LCC Reformulation

Denote $\bar{u}_{[1,T]}^d = [\bar{u}^d(1), \dots, \bar{u}^d(T)]^\top$ as the corresponding acceleration sequence of $u_{[1,T]}^d$ under the affine map (P_u, L_u) , and $\bar{y}_{[1,T]}^d = [\bar{y}^d(1), \dots, \bar{y}^d(T)]^\top$ as the corresponding output sequence of $y_{[1,T]}^d$ under the affine map (P_y, L_y) . Then, similar to $\hat{u}_{[1,T]}^d$, the combined input sequence $\hat{\bar{u}}_{[1,T]}^d \in \mathbb{R}^{(m+1)T}$ is constructed with $\bar{u}_{[1,T]}^d$ and $\epsilon_{[1,T]}^d$. The matrices $(\bar{U}_p^H, \bar{U}_f^H, \bar{Y}_p^H, \bar{Y}_f^H)$ and $(\bar{U}_p^P, \bar{U}_f^P, \bar{Y}_p^P, \bar{Y}_f^P)$ can be constructed with $\bar{u}_{[1,T]}^d$ and $\bar{y}_{[1,T]}^d$ by following the same procedure shown in (8) and (10), respectively. Motivated by Willems' fundamental lemma [28], (9) and (11), we use the data $(\bar{u}_{[1,T]}^d, \epsilon_{[1,T]}^d, \bar{y}_{[1,T]}^d)$ to represent the affine masking-based mixed traffic system (16) under the Hankel and Page matrix structures. The results are summarized below.

Proposition 3: Suppose the data $\hat{\bar{u}}_{[1,T]}^d$ is Hankel exciting of order $T_{\text{ini}} + N + 2n + 1$. Then, any trajectory $(\bar{u}_{\text{ini}}, \epsilon_{\text{ini}}, \bar{y}_{\text{ini}}, \bar{u}, \epsilon, \bar{y})$ of (16) can be constructed via

$$\begin{bmatrix} \bar{U}_p^H \\ E_p^H \\ \bar{Y}_p^H \\ \bar{U}_f^H \\ E_f^H \\ \bar{Y}_f^H \\ 1_{T-T_{\text{ini}}-N+1}^\top \end{bmatrix} \bar{g} = \begin{bmatrix} \bar{u}_{\text{ini}} \\ \epsilon_{\text{ini}} \\ \bar{y}_{\text{ini}} \\ \bar{u} \\ \epsilon \\ \bar{y} \\ 1 \end{bmatrix}, \quad (17)$$

where $\bar{g} \in \mathbb{R}^{T-T_{\text{ini}}-N+1}$.

Proof: See Appendix A. ■

Proposition 4: Suppose the data $\hat{\bar{u}}_{[1,T]}^d$ is $(T_{\text{ini}} + N)$ -Page exciting of order $2n + 2$. Then, any trajectory $(\bar{u}_{\text{ini}}, \epsilon_{\text{ini}}, \bar{y}_{\text{ini}}, \bar{u}, \epsilon, \bar{y})$ of (16) can be constructed via

$$\begin{bmatrix} \bar{U}_p^P \\ E_p^P \\ \bar{Y}_p^P \\ \bar{U}_f^P \\ E_f^P \\ \bar{Y}_f^P \\ 1_{\lfloor \frac{T}{T_{\text{ini}}+N} \rfloor}^\top \end{bmatrix} \bar{g} = \begin{bmatrix} \bar{u}_{\text{ini}} \\ \epsilon_{\text{ini}} \\ \bar{y}_{\text{ini}} \\ \bar{u} \\ \epsilon \\ \bar{y} \\ 1 \end{bmatrix}, \quad (18)$$

where $\bar{g} \in \mathbb{R}^{\lfloor \frac{T}{T_{\text{ini}}+N} \rfloor}$.

Proof: See Appendix B. ■

Remark 3: Propositions 1 and 2 work for standard LTI system (6), while Propositions 3 and 4 are extended to LTI system (16) with non-zero offsets \bar{L}_u and L_y . One key difference between Propositions 1/2 and 3/4 is the persistent excitation condition on $\hat{u}_{[1,T]}^d$. Proposition 1/2 requires $\hat{u}_{[1,T]}^d$

to be Hankel exciting of order $T_{\text{ini}} + N + 2n$ ($(T_{\text{ini}} + N)$ -Page exciting of order $2n + 1$), while Proposition 3/4 imposes that $\hat{u}_{[1,T]}^d$ is Hankel exciting of order $T_{\text{ini}} + N + 2n + 1$ ($(T_{\text{ini}} + N)$ -Page exciting of order $2n + 2$). The latter introduces an additional order to handle the constraint $1_{T-T_{\text{ini}}-N+1}^\top \bar{g} = 1$ ($1_{\lfloor \frac{T}{T_{\text{ini}}+N} \rfloor}^\top \bar{g} = 1$). This constraint ensures that the offsets \bar{L}_u and \bar{L}_y will be carried through from the pre-collected data $(\bar{u}^d, \epsilon^d, \bar{y}^d)$ to the trajectory $(\bar{u}_{\text{ini}}, \epsilon_{\text{ini}}, \bar{y}_{\text{ini}}, \bar{u}, \epsilon, \bar{y})$. Similar constraints can be found in [46] and [47]. \square

The affine maps are able to mask the true system state $x_i(k)$ and input $u_i(k)$ of CAVs to protect the privacy, and in the central unit, a new optimization problem with respect to (\bar{y}, \bar{u}) and the new non-parametric representation (17) (or (18)) are solved. Specifically, with the affine maps, one can show that (12) can be transformed into the following problem:

$$\begin{aligned} & \min_{\bar{g}, \bar{u}, \bar{y}} \bar{J}(\bar{y}, \bar{u}) \\ \text{s.t. } & (17) \text{ (or } (18)), \\ & \epsilon = 0_N, \\ & \bar{y}_{\min} \leq \bar{y}(k) \leq \bar{y}_{\max}, \quad k = t, \dots, t + N - 1, \\ & \bar{a}_{\min} \leq \bar{u}(k) \leq \bar{a}_{\max}, \quad k = t, \dots, t + N - 1, \end{aligned} \quad (19)$$

where the cost function is defined as

$$\bar{J}(\bar{y}, \bar{u}) = \sum_{k=t}^{t+N-1} \left(\|\bar{y}(k)\|_{\bar{Q}}^2 + \bar{q}^\top \bar{y}(k) + \|\bar{u}(k)\|_{\bar{R}}^2 + \bar{r}^\top \bar{u}(k) \right)$$

with $\bar{Q} \in \mathbb{R}^{(n+m) \times (n+m)}$, $\bar{q} \in \mathbb{R}^n$, $\bar{R} \in \mathbb{R}^{m \times m}$, $\bar{r} \in \mathbb{R}^m$, $\bar{Q}_f \in \mathbb{R}^{n \times n}$, and $\bar{q}_f \in \mathbb{R}^n$ given by

$$\begin{aligned} \bar{Q} &= P_y^{-\top} Q P_y^{-1} \in \mathbb{R}^{(n+m) \times (n+m)}, \bar{q} = -2\bar{Q}L_y \in \mathbb{R}^{(n+m)}, \\ \bar{R} &= P_u^{-\top} R P_u^{-1} \in \mathbb{R}^{m \times m}, \bar{r} = -2\bar{R}L_u \in \mathbb{R}^m. \end{aligned} \quad (20)$$

In (19), $(\bar{y}_{\min}, \bar{y}_{\max})$ and $(\bar{u}_{\min}, \bar{u}_{\max})$ are the corresponding constraint bounds of (y_{\min}, y_{\max}) and (u_{\min}, u_{\max}) under the affine maps (P_y, L_y) and (P_u, L_u) given in (15), i.e., $\bar{y}_{\min} = P_y y_{\min} + L_y$, $\bar{y}_{\max} = P_y y_{\max} + L_y$ and $\bar{u}_{\min} = P_u u_{\min} + L_u$, $\bar{u}_{\max} = P_u u_{\max} + L_u$.

Compared to the unsecure DeeP-LCC in Section IV-A, our privacy-preserved DeeP-LCC architecture with the affine maps, shown in Fig. 4, is modified as:

- *Handshaking Phase*: The vehicle system sends

$$\{\bar{Q}, \bar{R}, \bar{q}, \bar{r}, (\bar{u}_{[1,T]}^d, \epsilon_{[1,T]}^d, \bar{y}_{[1,T]}^d), (\bar{y}_{\min}, \bar{y}_{\max}, \bar{a}_{\min}, \bar{a}_{\max})\}$$

to the central unit, that is, the necessary information to set up the optimization problem (19).

- *Execution Phase*: At each time step k , the CAVs encodes $x_i(k)$ ($i \in \Omega_C$) into $\bar{x}_i(k)$ with $(P_{x,i}, l_{x,i})$ and sends $\bar{x}_i(k)$ to the central unit. Meanwhile, HDVs sends velocity error $\tilde{v}_i(k)$ ($i \in \Omega_H$) to the central unit. After receiving these data, the central unit computes $\bar{u}(k)$ by solving the optimization problem (19) and sends the solution $\bar{u}_i(k)$ ($i \in \Omega_C$) to the CAVs. Finally, each CAV uses $(P_{u,i}, l_{u,i})$ to decode $\bar{u}_i(k)$, i.e., $u_i(k) = P_{u,i}^{-1}(\bar{u}_i(k) - l_{u,i})$ and applies $u_i(k)$ to the actuators. The system then evolves over one step.

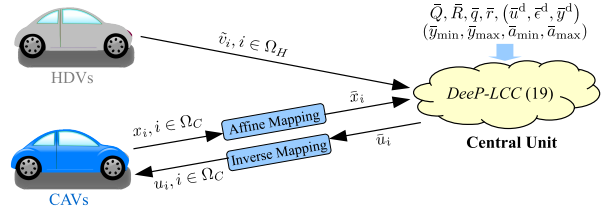


Fig. 4. Privacy-preservation DeeP-LCC architecture.

Note that during the handshaking phase, the information received by the central unit does not include affine maps (P_y, L_y) and (P_u, L_u) , and each CAV will not share its local affine map $(P_{u,i}, l_{u,i})$ with others during the execution phase. Therefore, the attackers are unable to infer the privacy-sensitive information $x_i(k)$ and $u_i(k)$. Rigorous definition and analysis of privacy preservation will be provided in Section V-B.

Remark 4: The formulations (17) and (18) are valid for deterministic LTI system (16). However, in practice, the car-following behavior of HDVs is stochastic and has uncertainties, which leads to a non-deterministic and nonlinear mixed traffic system. Inspired by the regularization design for standard DeePC [26], slack variable $\bar{\sigma}_y \in \mathbb{R}^{(n+m)T_{\text{ini}}}$ and two-norm regularization on \bar{g} can be introduced to handle system uncertainties and nonlinearities. For instance, the optimization problem (19) under the Hankel matrix structure becomes

$$\begin{aligned} & \min_{\bar{g}, \bar{u}, \bar{y}} \bar{J}(\bar{y}, \bar{u}) + \bar{\lambda}_g \|\bar{g}\|_2^2 + \bar{\lambda}_\sigma \|\bar{\sigma}_y\|_2^2 \\ \text{s.t. } & \begin{bmatrix} \bar{U}_p \\ \bar{E}_p \\ \bar{Y}_p \\ \bar{U}_f \\ \bar{E}_f \\ \bar{Y}_f \\ 1_{T-T_{\text{ini}}-N+1} \end{bmatrix} \bar{g} = \begin{bmatrix} \bar{u}_{\text{ini}} \\ \epsilon_{\text{ini}} \\ \bar{y}_{\text{ini}} \\ \bar{u} \\ \epsilon \\ \bar{y} \\ 1 \end{bmatrix} + \begin{bmatrix} 0 \\ 0 \\ \bar{\sigma}_y \\ 0 \\ 0 \\ 0 \\ 0 \end{bmatrix}, \\ & \epsilon = 0_N, \\ & \bar{y}_{\min} \leq \bar{y}(k) \leq \bar{y}_{\max}, \quad k = t, \dots, t + N - 1, \\ & \bar{a}_{\min} \leq \bar{u}(k) \leq \bar{a}_{\max}, \quad k = t, \dots, t + N - 1, \end{aligned} \quad (21)$$

where $\bar{\lambda}_g > 0$ and $\bar{\lambda}_\sigma > 0$ are weighting coefficients. The slack variable $\bar{\sigma}_y$ for the past output signal is added to ensure the feasibility of the equality constraint, while the regularization on \bar{g} is used to avoid overfitting. \square

V. EQUIVALENCE AND PRIVACY PRESERVATION

As mentioned in Section IV-A, the attacker aims to infer the system state and input of CAVs, i.e., $x_i(k) = [\tilde{s}_i(k), \tilde{v}_i(k)]^\top$, $u_i(k)$, $i \in \Omega_C$. Note that under the privacy-preserving DeeP-LCC architecture, the exchanged information between CAVs and the central unit during the execution phase is $\bar{x}_i(k)$ and $\bar{u}_i(k)$ rather than the actual system state and input. In the section, we first prove that the reformulated DeeP-LCC problem (19) is equivalent to the original DeeP-LCC problem (12), and then we show that the privacy of CAVs' state and input is indeed protected.

A. Equivalence With Affine Transformation

The following Lemma establishes that the equivalence of the reformulated DeeP-LCC problem (19) to the original DeeP-LCC problem (12).

Lemma 1: Under the affine transformation mechanism, the optimization problem (19) is equivalent to (12).

Proof: With the input and output transformations in (15), the cost term transformations in (20), and the definitions of $J(\cdot, \cdot)$ and $\bar{J}(\cdot, \cdot)$, it can be shown that

$$J(y, u) = \bar{J}(\bar{y}, \bar{u}) + \varrho, \quad (22)$$

where $\varrho = \sum_{k=t}^{t+N-1} (L_y^\top \bar{Q} L_y + L_u^\top \bar{R} L_u) \in \mathbb{R}$ is a constant. We now use proof by contradiction. Assume that (\bar{y}^*, \bar{u}^*) is the global minimizer of optimization problem (19), and (y^*, u^*) is the corresponding sequence of (\bar{y}^*, \bar{u}^*) under the inverse affine maps (P_y, L_y) , (P_u, L_u) , i.e.,

$$\begin{aligned} y^* &= \begin{bmatrix} y^*(t) \\ \vdots \\ y^*(t+N-1) \end{bmatrix} = \begin{bmatrix} P_y^{-1}(y^*(t) - L_y) \\ \vdots \\ P_y^{-1}(y^*(t+N-1) - L_y) \end{bmatrix}, \\ u^* &= \begin{bmatrix} u^*(t) \\ \vdots \\ u^*(t+N-1) \end{bmatrix} = \begin{bmatrix} P_u^{-1}(u^*(t) - L_u) \\ \vdots \\ P_u^{-1}(u^*(t+N-1) - L_u) \end{bmatrix}. \end{aligned}$$

As (\bar{y}^*, \bar{u}^*) is a trajectory of system (16) and satisfies the constraints in (19), it can be confirmed that (y^*, u^*) is a trajectory of system (6) and satisfies the constraints in (12). We also assume that (y^*, u^*) is not the global minimizer of problem (12), and thus there exists an optimal sequence (y^{**}, u^{**}) (other than (y^*, u^*)) such that

$$J(y^{**}, u^{**}) < J(y^*, u^*). \quad (23)$$

Let $(\bar{y}^{**}, \bar{u}^{**})$ be the corresponding trajectory of (y^{**}, u^{**}) under the forward affine maps (P_y, L_y) , (P_u, L_u) . According to (22), (23) can be rewritten as

$$\bar{J}(\bar{y}^{**}, \bar{u}^{**}) + \varrho < \bar{J}(\bar{y}^*, \bar{u}^*) + \varrho, \quad (24)$$

which contradicts the assumption that (\bar{y}^*, \bar{u}^*) is the global minimizer of optimization problem (19).

Therefore, if (\bar{y}^*, \bar{u}^*) is the global minimizer of problem (19), then its inverse affine transformation, i.e., (y^*, u^*) , should be solution to the original problem (12), indicating that these two problems are equivalent. ■

B. Privacy Preservation

We next discuss the privacy notion used in this paper. As mentioned in Section IV-A, the attacker aims to infer the system state $x_i(k)$ and control input $u_i(k)$ of CAVs. Under the privacy-preserving architecture discussed above, the attacker will have access to $\bar{x}_i(k)$ and $\bar{u}_i(k)$ at each time step k , and we need to show that for any $\kappa \in \mathbb{Z}_+$, $x_{i,[1,\kappa]}$ and $u_{i,[1,\kappa]}$ cannot be identified from $\bar{x}_{i,[1,\kappa]}$ and $\bar{u}_{i,[1,\kappa]}$. According to (13), we use

$$(x_{i,[1,\kappa]}, u_{i,[1,\kappa]}) \xrightarrow{(P_{x,i}, l_{x,i}, P_{u,i}, l_{u,i})} (\bar{x}_{i,[1,\kappa]}, \bar{u}_{i,[1,\kappa]}), \quad \forall i \in \Omega_C$$

to denote that $(\bar{x}_{i,[1,\kappa]}, \bar{u}_{i,[1,\kappa]})$ is the transformed trajectory of $(x_{i,[1,\kappa]}, u_{i,[1,\kappa]})$ under the affine maps $(P_{x,i}, l_{x,i})$ and $(P_{u,i}, l_{u,i})$.

For any feasible state sequence $\bar{x}_{i,[1,\kappa]}$ and input sequence $\bar{u}_{i,[1,\kappa]}$ received by the attacker, the set $\Delta(\bar{x}_{i,[1,\kappa]}, \bar{u}_{i,[1,\kappa]})$ is defined as

$$\begin{aligned} \Delta(\bar{x}_{i,[1,\kappa]}, \bar{u}_{i,[1,\kappa]}) &= \{x_{i,[1,\kappa]}, u_{i,[1,\kappa]} : \exists (P_{x,i}, l_{x,i}, P_{u,i}, l_{u,i}) \\ &\text{s.t. } (x_{i,[1,\kappa]}, u_{i,[1,\kappa]}) \xrightarrow{(P_{x,i}, l_{x,i}, P_{u,i}, l_{u,i})} (\bar{x}_{i,[1,\kappa]}, \bar{u}_{i,[1,\kappa]})\}. \end{aligned}$$

Essentially, the set $\Delta(\bar{x}_{i,[1,\kappa]}, \bar{u}_{i,[1,\kappa]})$ includes all possible values of $(x_{i,[1,\kappa]}, u_{i,[1,\kappa]})$ that can be transformed into $(\bar{x}_{i,[1,\kappa]}, \bar{u}_{i,[1,\kappa]})$ with corresponding affine maps $(P_{x,i}, l_{x,i}, P_{u,i}, l_{u,i})$.

Definition 2 (∞ -Diversity): The privacy of the actual system state $x_{i,[1,\kappa]}$ and input $u_{i,[1,\kappa]}$ of CAVs is preserved if the cardinality of the set $\Delta(\bar{x}_{i,[1,\kappa]}, \bar{u}_{i,[1,\kappa]})$ is infinite for any feasible state sequence $\bar{x}_{i,[1,\kappa]}$ and input sequence $\bar{u}_{i,[1,\kappa]}$.

The ∞ -Diversity privacy definition requires that there are infinite sets of $(x_{i,[1,\kappa]}, u_{i,[1,\kappa]})$ and $(P_{x,i}, l_{x,i}, P_{u,i}, l_{u,i})$ that can generate the same $(\bar{x}_{i,[1,\kappa]}, \bar{u}_{i,[1,\kappa]})$ received by the attacker. As a result, it is impossible for the attacker to use $(\bar{x}_{i,[1,\kappa]}, \bar{u}_{i,[1,\kappa]})$ to infer the actual system state and input information.

Remark 5: Definition 2 of ∞ -Diversity can be viewed as an extension to the l -diversity [48] that has been widely adopted in formal privacy analysis on attribute privacy of tabular. Essentially, l -diversity requires that there are at least l different possible values for the privacy-sensitive data attributes, and a greater l indicates greater indistinguishability. □

We next show that the proposed affine transformation mechanism can protect the privacy of CAVs based on Definition 2.

Theorem 1: Under the affine masking mechanism described in Section IV-B, the system state and control input of CAVs are ∞ -Diversity, that is, the attacker cannot infer the actual system state $x_i(k)$ and input $u_i(k)$, $\forall i \in \Omega_C$.

Proof: Based on Definition 2, we prove Theorem 1 by showing that under the affine masking scheme, the cardinality of the set $\Delta(\bar{x}_{i,[1,\kappa]}, \bar{u}_{i,[1,\kappa]})$ is infinite. Specifically, given the sequence $(\bar{x}_{i,[1,\kappa]}, \bar{u}_{i,[1,\kappa]})$ accessible to the attacker, for an arbitrary affine map $(P'_{x,i}, l'_{x,i}, P'_{u,i}, l'_{u,i})$ such that $P'_{x,i}$ and $P'_{u,i}$ are invertible, a sequence $(x'_{i,[1,\kappa]}, u'_{i,[1,\kappa]})$ can be uniquely determined based on $(\bar{x}_{i,[1,\kappa]}, \bar{u}_{i,[1,\kappa]})$ by using $(P'_{x,i}, l'_{x,i}, P'_{u,i}, l'_{u,i})$ as an inverse mapping. As there exists infinitely many such affine maps $(P'_{x,i}, l'_{x,i}, P'_{u,i}, l'_{u,i})$, there exist infinitely many $(x'_{i,[1,\kappa]}, u'_{i,[1,\kappa]})$ such that via proper affine transformations, the attacker will receive the same accessed information: $(\bar{x}_{i,[1,\kappa]}, \bar{u}_{i,[1,\kappa]})$, which indicates that the cardinality of the set $\Delta(\bar{x}_{i,[1,\kappa]}, \bar{u}_{i,[1,\kappa]})$ is infinite. ■

Remark 6: Different from the conventional encryption-based techniques [49], [50], the proposed affine masking-based privacy-preserved scheme does not involve complicated encryption and decryption procedure, and thus is light-weight in computation and can be easily implemented in a mixed traffic system. Furthermore, the affine masking mechanism can provide strong privacy protection such that the eavesdropper

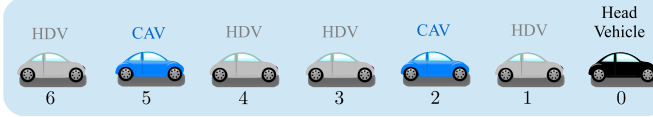


Fig. 5. Mixed traffic system for simulation.

TABLE I
PARAMETER SETUP FOR DEEP-LCC (12)

Notation	Meaning	Value
N	Length for future data horizon	30
T_{ini}	Length for past data horizon	15
w_s	Weight coefficient for spacing error	0.5
w_v	Weight coefficient for velocity error	1
w_u	Weight coefficient for control input	0.1
\tilde{s}_{\min} [m]	Lower bound of spacing error	-15
\tilde{s}_{\max} [m]	Upper bound of spacing error	20
\tilde{v}_{\min} [m/s]	Lower bound of velocity error	-30
\tilde{v}_{\max} [m/s]	Upper bound of velocity error	30
a_{\min} [m/s ²]	Lower bound of acceleration	-5
a_{\max} [m/s ²]	Upper bound of acceleration	2

cannot even approximately estimate the interested information $x_i(k)$ and $u_i(k)$ via the exchanged information between the vehicle system and the central unit. \square

VI. NUMERICAL EXPERIMENTS

In this section, we perform numerical simulations to validate the efficacy of the proposed privacy-preserving DeeP-LCC. Our implementation is adapted from the open-source code at <https://github.com/soc-ucsd/DeeP-LCC>. As shown in Fig. 5, we consider a mixed traffic system consisting of two CAVs, four HDVs, and one head vehicle. The CAV and HDV indices are $\Omega_C = \{2, 5\}$ and $\Omega_H = \{1, 3, 4, 6\}$, respectively. As discussed in Section IV, there exists a communication network between the central unit and vehicles. The central unit collects the vehicle data and then computes the control actions for the CAVs.

The OVM model [14] is used to describe the behavior of HDVs, and noises with uniform distribution of $\mathbb{U}[-0.3, 0.3]$ are added to the HDVs' model. Note that the OVM model is only used to update the state of HDVs and is not utilized by the developed control scheme. Both the original DeeP-LCC and the proposed privacy-preserving DeeP-LCC are implemented in the numerical simulations. We follow a similar procedure introduced in [24] to collect the offline data (u^d, ϵ^d, y^d) with the sampling interval chosen as $\Delta t = 0.05$ s. For the DeeP-LCC (12), the parameter setup is listed in Table I. For the proposed privacy-preserving DeeP-LCC, CAVs exploit affine transformation maps (13) to mask their actual state and input. The affine transformation maps for CAVs (recall that $\Omega_C = \{2, 5\}$) are chosen as

$$P_{x,2} = \begin{bmatrix} \cos(\frac{\pi}{4}) & -\sin(\frac{\pi}{4}) \\ \sin(\frac{\pi}{4}) & \cos(\frac{\pi}{4}) \end{bmatrix}, l_{x,2} = \begin{bmatrix} 5 \\ 3 \end{bmatrix},$$

$$P_{u,2} = -1.5, l_{u,2} = 1,$$

and

$$P_{x,5} = \begin{bmatrix} \cos(\frac{8\pi}{9}) & -\sin(\frac{8\pi}{9}) \\ \sin(\frac{8\pi}{9}) & \cos(\frac{8\pi}{9}) \end{bmatrix}, l_{x,5} = \begin{bmatrix} 5 \\ 3 \end{bmatrix},$$

$$P_{u,5} = 1.5, l_{u,5} = -1.$$

Furthermore, based on the aforementioned affine maps and the parameter setup for DeeP-LCC, the parameters used to formulate the privacy-preserving DeeP-LCC problem 19 can be obtained (see Section IV-B and IV-C).

A. Scenario A: Comprehensive Acceleration and Deceleration

Motivated by the New European Driving Cycle (NEDC) [51] and the experiments in [24], a comprehensive acceleration and deceleration scenario is designed to validate the capability of the proposed privacy-preserving DeeP-LCC in improving traffic performance. The NEDC combines ECE 15 with Extra Urban Driving Cycle (EUDC) to assess the fuel economy of vehicles. Similar to ECE 15 and EUDC, we design a driving trajectory for the head vehicle that incorporates acceleration and deceleration at different time periods. Both fuel consumption and velocity errors for the vehicles are considered to quantify traffic performance.

More specifically, for the i -th vehicle, the fuel consumption rate f_i (mL/s) is calculated based on an instantaneous model in [52], which is given by

$$f_i = \begin{cases} 0.444 + 0.090 R_i v_i + \left[0.054 a_i^2 v_i \right]_{a_i > 0}, & \text{if } R_i > 0, \\ 0.444, & \text{if } R_i \leq 0, \end{cases}$$

with $R_i = 0.333 + 0.00108 v_i^2 + 1.200 a_i$. Since the first HDV is not influenced by the CAVs, the total fuel consumption rate f of the mixed traffic system is calculated by summing f_i indexed from 2 to 6, i.e., $f = \sum_{i=2}^6 f_i$. The average absolute velocity error (AAVE) is utilized to quantify velocity errors and is obtained by computing the average of $\frac{|v_i(t) - v_0(t)|}{v_0(t)}$ with respect to the simulation time and the vehicle number. Moreover, the original DeeP-LCC scheme and the proposed privacy-preserving DeeP-LCC under the Hankel and Page matrix structures are tested in this scenario. The number of columns in Hankel and Page matrices are selected as 900, which is sufficient for the non-parametric representation of the mixed traffic system with 2 CAVs and 4 HDVs. A standard output-feedback MPC is also tested in this scenario to facilitate a complete comparison. The MPC is designed based on the linearized mixed traffic system model (6), and its future time horizon, cost function, and constraints are the same as those of DeeP-LCC. Each method is carried out one time in this scenario, and the fuel consumption and AAVE indices are computed to evaluate the performance.

The simulation results are shown in Fig. 6. Note that the velocity response profiles of MPC and Page matrix based DeeP-LCC schemes are quite similar to the ones of Hankel matrix based DeeP-LCC schemes, and hence they are omitted. As shown in Fig. 6, compared to the case with all HDVs, both the original DeeP-LCC and the proposed privacy-preserving DeeP-LCC can effectively mitigate velocity fluctuations, leading to a smoother mixed traffic flow. Table II presents the fuel consumption and AAVE of different schemes. All DeeP-LCC approaches achieve comparable performance with the ideal MPC setting. Note that MPC relies on the nominal

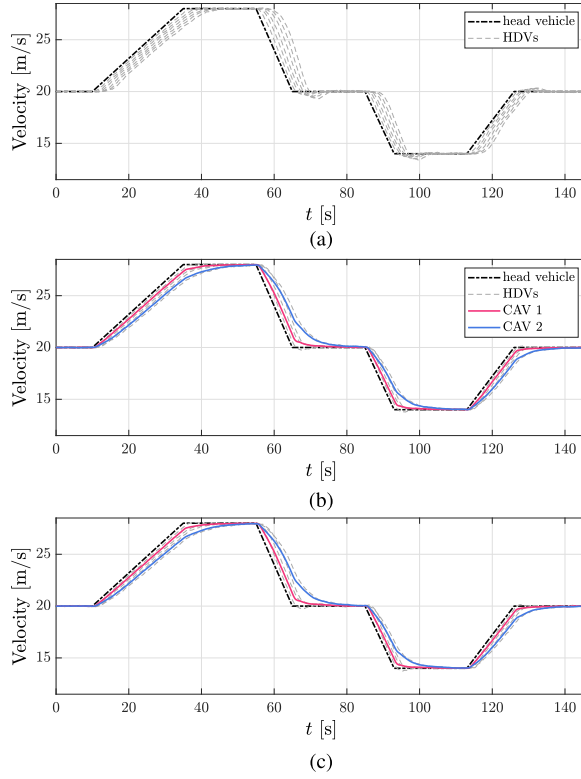


Fig. 6. Velocity profiles of the mixed traffic system under Scenario A. (a) All the vehicles are HDVs. (b) DeeP-LCC under the Hankel matrix structure is utilized to generate the control for CAVs. (c) Privacy-preserving DeeP-LCC under the Hankel matrix structure is utilized to generate the control for CAVs.

model (6) to facilitate the controller design (that is generally not available), while DeeP-LCC approaches directly utilize pre-collected trajectory data to generate control inputs. The explicit model for each HDV is generally unknown and hard to identify due to stochastic and uncertain human driving behavior, and thus MPC is not easily applicable to real-world deployment. In contrast, DeeP-LCC approaches can bypass system identification and accomplish similar performance with MPC based on pre-collected data, which might be easier to deploy for mixed traffic with enhanced communication technologies.

In addition, it can be found from Table II that the proposed privacy-preserving method still retains the advantages of the original DeeP-LCC in improving fuel economy and traffic smoothness. As revealed in Lemma 1, although the affine transformation mechanism is introduced to mask the actual system state and input signals, the resulting privacy-preserving DeeP-LCC (19) is equivalent to the original DeeP-LCC (12). Therefore, the proposed privacy protection scheme is shown not to induce degradation on control performance.

Both the original DeeP-LCC (12) and the privacy-preserving DeeP-LCC (19) can be formulated into a standard quadratic program, and the dimension of their main decision variables g/\bar{g} is identical to the column number of data matrix. In this simulation, both Hankel and Page matrices have the same column number of 900, i.e., $g, \bar{g} \in \mathbb{R}^{900}$. For MPC, its main decision variable is the future control sequence, which has the size of $N \times m = 60$. Therefore, the online optimization complexity of DeeP-LCC approaches is higher than that of

TABLE II
FUEL CONSUMPTION AND AVERAGE ABSOLUTE VELOCITY ERROR (AAVE) IN SCENARIO A

	Fuel Consumption [mL]	AAVE [10^{-3}]
All HDVs	1569.62	27.34
MPC	1536.98($\downarrow 2.08\%$)	24.50($\downarrow 10.38\%$)
DeeP-LCC (Hankel)	1537.98($\downarrow 2.02\%$)	24.52($\downarrow 10.29\%$)
PP-DeeP-LCC (Hankel)	1538.71($\downarrow 1.97\%$)	24.48($\downarrow 10.47\%$)
DeeP-LCC (Page)	1537.66($\downarrow 2.07\%$)	24.48($\downarrow 10.45\%$)
PP-DeeP-LCC (Page)	1538.73($\downarrow 1.97\%$)	24.50($\downarrow 10.39\%$)

¹ All the values have been rounded. PP-DeeP-LCC refers to privacy-preserving DeeP-LCC.

TABLE III
VARIABLE DIMENSION AND COMPUTATION TIME IN SCENARIO A

	Decision Variable Dimension	Mean Computation Time [ms]
MPC	60	3.58
DeeP-LCC (Hankel)	900	26.31
PP-DeeP-LCC (Hankel)	900	27.71
DeeP-LCC (Page)	900	27.49
PP-DeeP-LCC (Page)	900	27.91

MPC. We run the MPC and DeeP-LCC approaches in a computer with Intel Core i7-12700K CPU and 16G RAM, and the computation time is concluded in Table III, which confirms that the DeeP-LCC approaches require more computation time than the MPC. However, without further customization or optimization of the code, the mean computation time of DeeP-LCC approaches during this simulation is less than 30 ms, which is acceptable for deployment in the considered mixed traffic system. Improving the computational efficiency of DeeP-LCC for large-scale system is an interesting future direction. We refer the interested readers to [53] and [54] for recent potential strategies based on dimension reduction and distributed optimization techniques.

B. Scenario B: Highway Vehicle Trajectory

In this scenario, the real vehicle trajectory from the Next Generation SIMulation (NGSIM) program [55] is used to further validate the proposed privacy-preserving DeeP-LCC scheme. The NGSIM program provides comprehensive high-quality traffic data collected from two freeway segments and two arterial segments. We use the traffic data collected on a freeway segment of US-101 to facilitate the simulation. In particular, four vehicle trajectories (i.e., No. 2, 22, 42, and 48) between 8:05 a.m. to 8:20 a.m. in the US-101 dataset are extracted and inputted as the head vehicle trajectory of the mixed traffic system. Fig. 7 shows the velocity profile of these four trajectories. All trajectories include significant oscillating procedure and thus are selected to validate the effectiveness of the proposed scheme in terms of fuel economy and traffic smoothness.

MPC and all DeeP-LCC related schemes are tested in this scenario, and the fuel consumption and AAVE indices are utilized to evaluate the performance. The performance improvement of MPC and DeeP-LCC approaches compared with the case where all the vehicles are HDVs is illustrated in Fig. 8. It is evident that MPC and all DeeP-LCC approaches

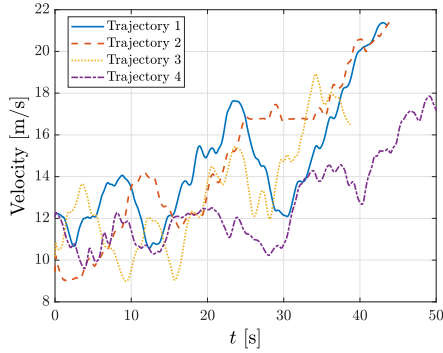


Fig. 7. Four vehicle trajectories from the NGSIM program. The trajectories are inputted as the head vehicle trajectory.

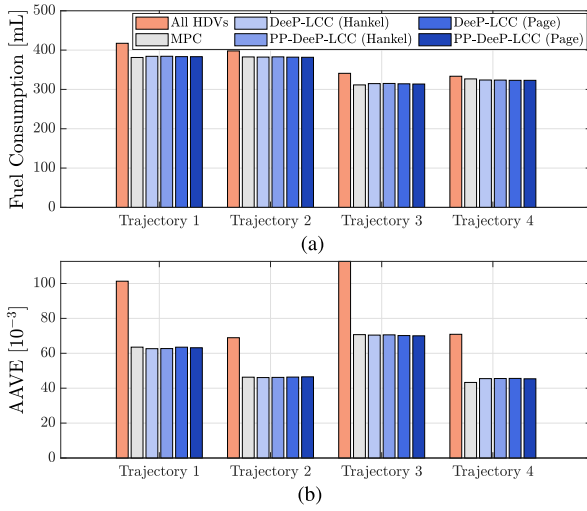


Fig. 8. Performance improvement of MPC and DeeP-LCC approaches compared with the case where all the vehicles are HDVs under Scenario B: (a) Fuel Consumption; and (b) AAVE.

substantially improve the fuel economy and traffic smoothness. Moreover, the improved traffic behavior under the proposed privacy-preserving DeeP-LCC is quite similar to that of the original DeeP-LCC, which indicates that the developed privacy protection method does not sacrifice traffic control efficacy for privacy.

C. Scenario C: Emergency Braking

We finally use a braking scenario to show that the proposed method can protect the privacy of CAVs against the attacker. In this scenario, the head vehicle takes a sudden emergency brake with maximum deceleration, then maintains the low velocity for a while, and finally accelerates to the original velocity. This is a typical emergency situation in real-world traffic, and the control actions of CAVs should provide strict safety guarantees to prevent rear-end collision.

The simulation results are presented in Figs. 9 and 10. It can be found from Fig. 9 that when all the vehicles are HDVs, their velocities have a large fluctuation in response to the head vehicle's braking perturbation. This velocity fluctuation will greatly increase fuel consumption and collision risk. By comparison, under the DeeP-LCC strategy and

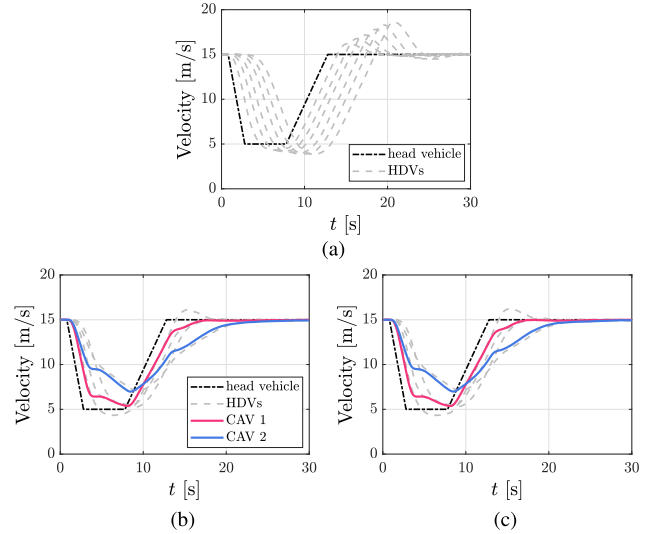


Fig. 9. Velocity profiles of the mixed traffic system under Scenario C. (a) All the vehicles are HDVs. (b) DeeP-LCC under the Page matrix structure is utilized to generate the control for CAVs. (c) Privacy-preserving DeeP-LCC under the Page matrix structure is utilized to generate the control for CAVs.

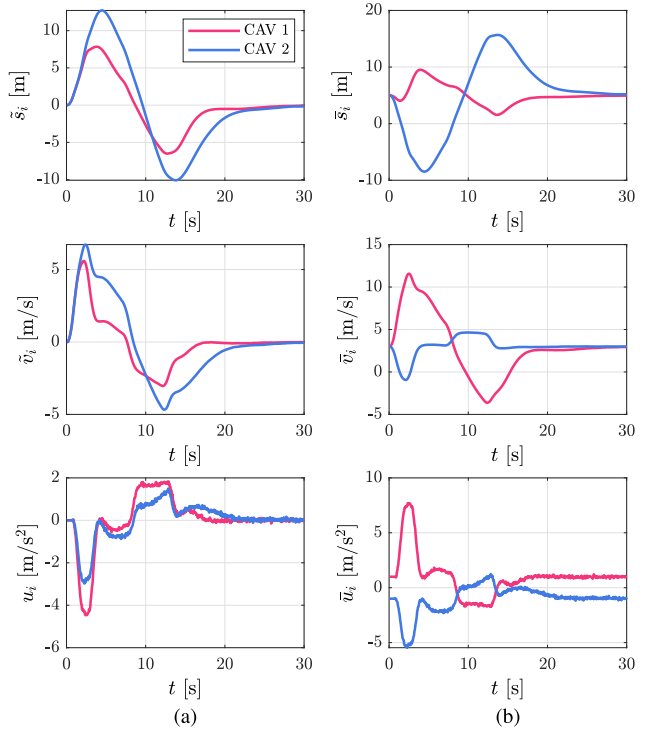


Fig. 10. Simulation results with privacy-preserving DeeP-LCC under Scenario C: (a) actual state and input information of CAVs, (b) state and input information exchanged between the CAVs and the central unit.

the proposed privacy-preserving DeeP-LCC, the CAVs show similar response patterns to mitigate velocity perturbations and smooth the mixed traffic flow. More precisely, when the head vehicle begins to brake (see the time period before 8 s), the CAVs decelerate immediately to adjust the relative distance from the preceding vehicle; when the head vehicle starts to return to the original velocity (see the time period after 8 s), the CAVs accelerate gradually. The similar motion pattern under these two methods implies that the affine transformation

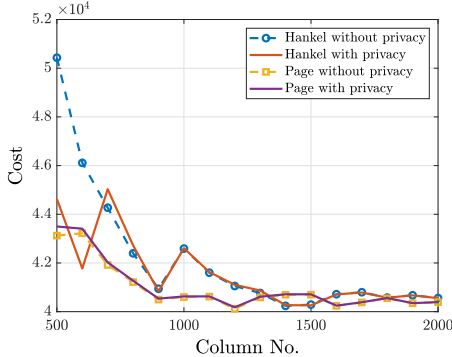


Fig. 11. Cost evolution under different number of columns in data matrix.

mechanism can retain the control performance as the original DeeP-LCC.

Recall that for the original DeeP-LCC architecture introduced in Section IV-A, each CAV needs to exchange real-time information with the central unit, which will directly leak privacy-sensitive messages $x_i(k)$ and $u_i(k)$ to the external eavesdropper or the honest-but-curious central unit. To avoid privacy leakage, we design a masking mechanism to modify the exchanged messages between the CAVs and the central unit. Fig. 10 shows the actual state and input information of CAVs (i.e., $x_i(k) = [\tilde{s}_i(k), \tilde{v}_i(k)]^\top, u_i(k), i \in \Omega_C$), and the corresponding modified information exchanged between the CAVs and the central unit (i.e., $\bar{x}_i(k) = [\bar{s}_i(k), \bar{v}_i(k)]^\top, \bar{u}_i(k), i \in \Omega_C$) under the privacy-preserving DeeP-LCC. It can be observed that the information exchanged between the CAVs and the central unit is quite different from the actual one. This indicates that the proposed affine transformation mechanism can conceal the actual state and input of CAVs, which makes the external eavesdropper or the honest-but-curious central unit unable to infer $x_i(k)$ and $u_i(k)$.

As discussed in Remark 2, the key difference between the Hankel matrix and the Page matrix is that there are no repeated entries in the latter. We conduct simulation to evaluate the performance of Hankel and Page matrix structures and analyze the effect of this difference. Specifically, with number of columns in data matrix ranging from 500 to 2000, the original DeeP-LCC without privacy protection and the proposed privacy-preserving DeeP-LCC are tested in Scenario B. The quadratic cost defined in (12) is calculated to evaluate the performance. Fig. 11 shows the cost of the mixed traffic system with different number of columns in Hankel and Page matrices. It can be seen that when the number of columns is less than 1300, compared to the Hankel matrix based DeeP-LCC, the Page matrix based ones show less cost volatility. Since none of the entries in the Page matrix are repeated, the Page matrix can store more data than the Hankel matrix with the same number of columns. More data samples generally contain more information about the system, hence the Page matrix based DeeP-LCC could be more efficient in representing the system via the non-parametric manner, resulting in lower cost fluctuations. When the number of columns is larger than 1300, both these two matrix structures store adequate

data, and thus the cost of Hankel matrix based DeeP-LCC and Page matrix based DeeP-LCC is stable around a constant.

VII. CONCLUSION

This paper has presented a privacy-preserving DeeP-LCC for CAVs in a mixed-traffic environment. We have considered external eavesdropper and honest-but-curious central unit who intend to infer the CAVs' system states and inputs. A simple yet effective affine transformation mechanism has been designed to enable privacy preservation, and an extended form of the data-enabled predictive control has been derived to achieve safe and optimal control for CAVs. The proposed affine transformation mechanism can be seamlessly integrated into the data-enabled control without affecting the control performance. Theoretical and simulation results confirm that by using the proposed method, the leading cruise control [10] in mixed traffic can be addressed while avoiding disclosing private information to the attacker.

There are several interesting future directions: first, the current privacy-preserving DeeP-LCC follows a centralized control fashion that may not be scalable, and thus distributed versions are worth further investigation for large-scale mixed traffic systems; second, it is very interesting to study mixed traffic control when there exist communication delays and/or only a portion of HDV data is accessible.

APPENDIX A PROOF OF PROPOSITION 3

Proof: If $(\bar{u}_{\text{ini}}, \epsilon_{\text{ini}}, \bar{y}_{\text{ini}}, \bar{u}, \epsilon, \bar{y})$ is a trajectory of (16) with initial state being $x(t - T_{\text{ini}})$, then the input-output response over $[t - T_{\text{ini}}, t + N - 1]$ can be expressed as

$$\begin{bmatrix} \bar{y}_{\text{ini}} \\ \bar{y} \end{bmatrix} = [\mathcal{T}_u \ \mathcal{T}_\epsilon \ \mathcal{T}_x \ \mathcal{T}_l] \begin{bmatrix} \bar{u}_{\text{ini}} \\ \bar{u} \\ \epsilon_{\text{ini}} \\ \epsilon \\ x(t - T_{\text{ini}}) \\ 1 \end{bmatrix}, \quad (25)$$

where the matrices $\mathcal{T}_u, \mathcal{T}_\epsilon, \mathcal{T}_x, \mathcal{T}_l$ are given by

$$\begin{aligned} \mathcal{T}_u &= \begin{bmatrix} 0 & 0 & 0 & \cdots & 0 \\ \bar{C}_d \bar{B}_d & 0 & 0 & \cdots & 0 \\ \bar{C}_d A_d \bar{B}_d & \bar{C}_d \bar{B}_d & 0 & \cdots & 0 \\ \vdots & \vdots & \vdots & \ddots & \vdots \\ \bar{C}_d A_d^{T_{\text{ini}}+N-2} \bar{B}_d & \bar{C}_d A_d^{T_{\text{ini}}+N-3} \bar{B}_d & \bar{C}_d A_d^{T_{\text{ini}}+N-4} \bar{B}_d & \cdots & 0 \end{bmatrix}, \\ \mathcal{T}_\epsilon &= \begin{bmatrix} 0 & 0 & 0 & \cdots & 0 \\ \bar{C}_d H_d & 0 & 0 & \cdots & 0 \\ \bar{C}_d A_d \bar{B}_d & \bar{C}_d \bar{B}_d & 0 & \cdots & 0 \\ \vdots & \vdots & \vdots & \ddots & \vdots \\ \bar{C}_d A_d^{T_{\text{ini}}+N-2} H_d & \bar{C}_d A_d^{T_{\text{ini}}+N-3} H_d & \bar{C}_d A_d^{T_{\text{ini}}+N-4} H_d & \cdots & 0 \end{bmatrix}, \\ \mathcal{T}_x &= \begin{bmatrix} \bar{C}_d \\ \bar{C}_d A_d \\ \vdots \\ \bar{C}_d A_d^{T_{\text{ini}}+N-1} \end{bmatrix}, \quad \mathcal{T}_l = \begin{bmatrix} L_y \\ L_y + \bar{C}_d \bar{L}_u \\ \vdots \\ L_y + \sum_{i=0}^{i=T_{\text{ini}}+N-2} \bar{C}_d A_d^i \bar{L}_u \end{bmatrix}. \end{aligned}$$

Considering that $(\bar{u}^d, \epsilon^d, \bar{y}^d)$ is a pre-collected trajectory of (16) and the definition of

$(\bar{Y}_p^{\mathcal{H}}, \bar{Y}_f^{\mathcal{H}}, \bar{U}_p^{\mathcal{H}}, \bar{U}_f^{\mathcal{H}}, E_p^{\mathcal{H}}, E_f^{\mathcal{H}})$, we derive that

$$\begin{bmatrix} \bar{Y}_p^{\mathcal{H}} \\ \bar{Y}_f^{\mathcal{H}} \end{bmatrix} = [T_u \ T_\epsilon \ T_x \ T_l] \begin{bmatrix} \bar{U}_p^{\mathcal{H}} \\ \bar{U}_f^{\mathcal{H}} \\ \hline E_p^{\mathcal{H}} \\ E_f^{\mathcal{H}} \\ \hline X_d^{\mathcal{H}} \\ \hline 1^\top_{T-T_{\text{ini}}-N+1} \end{bmatrix}, \quad (26)$$

where $X_d^{\mathcal{H}} = [x^d(1), x^d(2), \dots, x^d(T - T_{\text{ini}} - N + 1)] \in \mathbb{R}^{2n \times (T - T_{\text{ini}} - N + 1)}$.

We next show that the following matrix

$$\begin{bmatrix} \bar{U}_p^{\mathcal{H}} \\ \bar{U}_f^{\mathcal{H}} \\ \hline E_p^{\mathcal{H}} \\ E_f^{\mathcal{H}} \\ \hline X_d^{\mathcal{H}} \\ \hline 1^\top_{T-T_{\text{ini}}-N+1} \end{bmatrix} \quad (27)$$

has full row rank. It is clear that (16) can be rewritten as

$$\begin{bmatrix} x(k+1) \\ 1 \end{bmatrix} = \check{A}_d \begin{bmatrix} x(k) \\ 1 \end{bmatrix} + \check{B}_d \begin{bmatrix} \bar{u}(k) \\ \epsilon(k) \end{bmatrix}, \quad (28)$$

where

$$\check{A}_d = \begin{bmatrix} A_d & \bar{L}_u \\ 0 & 1 \end{bmatrix}, \quad \check{B}_d = \begin{bmatrix} \bar{B}_d & H_d \\ 0 & 0 \end{bmatrix}. \quad (29)$$

Let $[\eta_u, \eta_\epsilon, \xi_x, \xi_l]$ be a vector in the left kernel of (27), where $\eta_u^\top \in \mathbb{R}^{m(T_{\text{ini}}+N)}$, $\eta_\epsilon^\top \in \mathbb{R}^{T_{\text{ini}}+N}$, $\xi_x^\top \in \mathbb{R}^{2n}$, and $\xi_l \in \mathbb{R}$. Based on (27), (28), and the condition that $\hat{u}_{[1,T]}^d$, i.e., $(\bar{u}_{[1,T]}^d, \epsilon_{[1,T]}^d)$, is Hankel exciting of order $T_{\text{ini}}+N+2n+1$, we can follow the same arguments from the proof in [56, Theorem 1] to obtain that $\eta_u = 0$, $\eta_\epsilon = 0$, and

$$[\xi_x, \xi_l] \check{B}_d = [\xi_x, \xi_l] \check{A}_d \check{B}_d = \dots = [\xi_x, \xi_l] \check{A}_d^{2n} \check{B}_d = 0. \quad (30)$$

According to (29) and (30), it can be derived that

$$\xi_x [\bar{B}_d \ H_d] = \xi_x A_d [\bar{B}_d \ H_d] = \dots = \xi_x A_d^{2n} [\bar{B}_d \ H_d] = 0. \quad (31)$$

Since $(A_d, [B_d \ H_d])$ is controllable and $\bar{B}_d = B_d P_u^{-1}$, we can conclude that $(A_d, [\bar{B}_d \ H_d])$ is controllable. (31) and the controllability of $(A_d, [\bar{B}_d \ H_d])$ reveal that $\xi_x = 0$. Furthermore, as $[\eta_u, \eta_\epsilon, \xi_x, \xi_l]$ is a vector in the left kernel of (27), $\eta_u = 0$, $\eta_\epsilon = 0$, and $\xi_x = 0$, we have $\xi_l 1^\top_{T-T_{\text{ini}}-N+1} = 0$, indicating that $\xi_l = 0$. Based on $[\eta_u, \eta_\epsilon, \xi_x, \xi_l] = 0$, we can conclude that (27) has full row rank.

Based on the Rouché-Capelli theorem, the full row rank of (27) implies the existence of $\bar{g} \in \mathbb{R}^{T-T_{\text{ini}}-N+1}$ such that

$$\begin{bmatrix} \bar{u}_{\text{ini}} \\ \bar{u} \\ \hline \epsilon_{\text{ini}} \\ \epsilon \\ \hline x(t-T_{\text{ini}}) \\ \hline 1 \end{bmatrix} = \begin{bmatrix} \bar{U}_p^{\mathcal{H}} \\ \bar{U}_f^{\mathcal{H}} \\ \hline E_p^{\mathcal{H}} \\ E_f^{\mathcal{H}} \\ \hline X_d^{\mathcal{H}} \\ \hline 1^\top_{T-T_{\text{ini}}-N+1} \end{bmatrix} \bar{g}. \quad (32)$$

Substituting (26) and (32) into (25), it can be obtained that

$$\begin{bmatrix} \bar{y}_{\text{ini}} \\ \bar{y} \end{bmatrix} = \begin{bmatrix} \bar{Y}_p^{\mathcal{H}} \\ \bar{Y}_f^{\mathcal{H}} \end{bmatrix} \bar{g}. \quad (33)$$

From (32) and (33), it can be concluded that there exists \bar{g} such that (17) is satisfied, which completes the proof. ■

APPENDIX B PROOF OF PROPOSITION 4

Proof: According to the system dynamics and the definition of $(\bar{Y}_p^{\mathcal{P}}, \bar{Y}_f^{\mathcal{P}}, \bar{U}_p^{\mathcal{P}}, \bar{U}_f^{\mathcal{P}}, E_p^{\mathcal{P}}, E_f^{\mathcal{P}})$, we have

$$\begin{bmatrix} \bar{Y}_p^{\mathcal{P}} \\ \bar{Y}_f^{\mathcal{P}} \end{bmatrix} = [T_u \ T_\epsilon \ T_x \ T_l] \begin{bmatrix} \bar{U}_p^{\mathcal{P}} \\ \bar{U}_f^{\mathcal{P}} \\ \hline E_p^{\mathcal{P}} \\ E_f^{\mathcal{P}} \\ \hline X_d^{\mathcal{P}} \\ \hline 1^\top_{\lfloor \frac{T}{T_{\text{ini}}+N} \rfloor} \end{bmatrix}, \quad (34)$$

where

$$X_d^{\mathcal{P}} = \left[x^d(1), x^d(T_{\text{ini}}+N+1), \dots, x^d((\lfloor \frac{T}{T_{\text{ini}}+N} \rfloor - 1)(T_{\text{ini}}+N) + 1) \right] \in \mathbb{R}^{2n \times (\lfloor \frac{T}{T_{\text{ini}}+N} \rfloor)}.$$

By following the similar arguments from Theorem 2.1 in [23] and from Appendix A, it can be proved that if $\hat{u}_{[1,T]}^d$, i.e., $(\bar{u}_{[1,T]}^d, \epsilon_{[1,T]}^d)$, is $(T_{\text{ini}}+N)$ -Page exciting of order $2n+2$, then the following full row rank property is satisfied:

$$\text{rank} \begin{bmatrix} \bar{U}_p^{\mathcal{P}} \\ \bar{U}_f^{\mathcal{P}} \\ \hline E_p^{\mathcal{P}} \\ E_f^{\mathcal{P}} \\ \hline X_d^{\mathcal{P}} \\ \hline 1^\top_{\lfloor \frac{T}{T_{\text{ini}}+N} \rfloor} \end{bmatrix} = (m+1)(T_{\text{ini}}+N) + 2n + 1. \quad (35)$$

Based on (25), (34) and the rank condition (35), it can be concluded that there exists a vector $\bar{g} \in \mathbb{R}^{\lfloor \frac{T}{T_{\text{ini}}+N} \rfloor}$ such that

$$\begin{bmatrix} \bar{u}_{\text{ini}} \\ \bar{u} \\ \hline \epsilon_{\text{ini}} \\ \epsilon \\ \hline x(t-T_{\text{ini}}) \\ \hline 1 \end{bmatrix} = \begin{bmatrix} \bar{U}_p^{\mathcal{P}} \\ \bar{U}_f^{\mathcal{P}} \\ \hline E_p^{\mathcal{P}} \\ E_f^{\mathcal{P}} \\ \hline X_d^{\mathcal{P}} \\ \hline 1^\top_{\lfloor \frac{T}{T_{\text{ini}}+N} \rfloor} \end{bmatrix} \bar{g}, \quad (36)$$

and

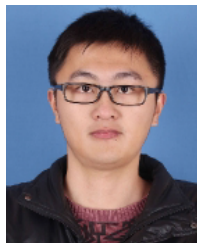
$$\begin{bmatrix} \bar{y}_{\text{ini}} \\ \bar{y} \end{bmatrix} = \begin{bmatrix} \bar{Y}_p^{\mathcal{P}} \\ \bar{Y}_f^{\mathcal{P}} \end{bmatrix} \bar{g}. \quad (37)$$

Finally, we can conclude from (36) and (37) that there exists \bar{g} such that (18) is satisfied. ■

REFERENCES

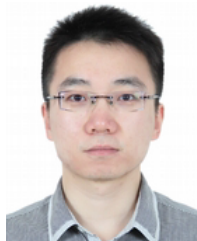
- [1] A. Vahidi and A. Sciarretta, "Energy saving potentials of connected and automated vehicles," *Transp. Res. C, Emerg. Technol.*, vol. 95, pp. 822–843, Oct. 2018.
- [2] S. E. Li et al., "Dynamical modeling and distributed control of connected and automated vehicles: Challenges and opportunities," *IEEE Intell. Transp. Syst. Mag.*, vol. 9, no. 3, pp. 46–58, Fall. 2017.
- [3] V. Milanés, S. E. Shladover, J. Spring, C. Nowakowski, H. Kawazoe, and M. Nakamura, "Cooperative adaptive cruise control in real traffic situations," *IEEE Trans. Intell. Transp. Syst.*, vol. 15, no. 1, pp. 296–305, Feb. 2014.
- [4] Y. Zheng, S. E. Li, K. Li, F. Borrelli, and J. K. Hedrick, "Distributed model predictive control for heterogeneous vehicle platoons under unidirectional topologies," *IEEE Trans. Control Syst. Technol.*, vol. 25, no. 3, pp. 899–910, May 2017.
- [5] C. Wang, S. Gong, A. Zhou, T. Li, and S. Peeta, "Cooperative adaptive cruise control for connected autonomous vehicles by factoring communication-related constraints," *Transp. Res. C, Emerg. Technol.*, vol. 113, pp. 124–145, Apr. 2020.
- [6] H. Guo, J. Liu, Q. Dai, H. Chen, Y. Wang, and W. Zhao, "A distributed adaptive triple-step nonlinear control for a connected automated vehicle platoon with dynamic uncertainty," *IEEE Internet Things J.*, vol. 7, no. 5, pp. 3861–3871, May 2020.
- [7] G. Orosz, "Connected cruise control: Modelling, delay effects, and nonlinear behaviour," *Vehicle Syst. Dyn.*, vol. 54, no. 8, pp. 1147–1176, Aug. 2016.
- [8] J. I. Ge and G. Orosz, "Optimal control of connected vehicle systems with communication delay and driver reaction time," *IEEE Trans. Intell. Transp. Syst.*, vol. 18, no. 8, pp. 2056–2070, Aug. 2017.
- [9] J. I. Ge, S. S. Avedisov, C. R. He, W. B. Qin, M. Sadeghpour, and G. Orosz, "Experimental validation of connected automated vehicle design among human-driven vehicles," *Transp. Res. C, Emerg. Technol.*, vol. 91, pp. 335–352, Jun. 2018.
- [10] J. Wang, Y. Zheng, C. Chen, Q. Xu, and K. Li, "Leading cruise control in mixed traffic flow: System modeling, controllability, and string stability," *IEEE Trans. Intell. Transp. Syst.*, vol. 23, no. 8, pp. 12861–12876, Aug. 2022.
- [11] S. Feng, Z. Song, Z. Li, Y. Zhang, and L. Li, "Robust platoon control in mixed traffic flow based on tube model predictive control," *IEEE Trans. Intell. Vehicles*, vol. 6, no. 4, pp. 711–722, Dec. 2021.
- [12] Y. Zheng, J. Wang, and K. Li, "Smoothing traffic flow via control of autonomous vehicles," *IEEE Internet Things J.*, vol. 7, no. 5, pp. 3882–3896, May 2020.
- [13] J. Wang, Y. Zheng, Q. Xu, J. Wang, and K. Li, "Controllability analysis and optimal control of mixed traffic flow with human-driven and autonomous vehicles," *IEEE Trans. Intell. Transp. Syst.*, vol. 22, no. 12, pp. 7445–7459, Dec. 2021.
- [14] M. Bando, K. Hasebe, A. Nakayama, A. Shibata, and Y. Sugiyama, "Dynamical model of traffic congestion and numerical simulation," *Phys. Rev. E, Stat. Phys. Plasmas Fluids Relat. Interdiscip. Top.*, vol. 51, no. 2, pp. 1035–1042, Feb. 1995.
- [15] M. Treiber, A. Hennecke, and D. Helbing, "Congested traffic states in empirical observations and microscopic simulations," *Phys. Rev. E, Stat. Phys. Plasmas Fluids Relat. Interdiscip. Top.*, vol. 62, no. 2, pp. 1805–1824, Aug. 2000.
- [16] T. Chu and U. Kalabac, "Model-based deep reinforcement learning for CACC in mixed-autonomy vehicle platoon," in *Proc. IEEE 58th Conf. Decis. Control (CDC)*, Dec. 2019, pp. 4079–4084.
- [17] E. Vinitsky, K. Parvate, A. Kreidieh, C. Wu, and A. Bayen, "Lagrangian control through deep-RL: Applications to bottleneck decongestion," in *Proc. 21st Int. Conf. Intell. Transp. Syst. (ITSC)*, Nov. 2018, pp. 759–765.
- [18] D. Chen et al., "Deep multi-agent reinforcement learning for highway on-ramp merging in mixed traffic," *IEEE Trans. Intell. Transp. Syst.*, early access, Jun. 22, 2023, doi: [10.1109/TITS.2023.3285442](https://doi.org/10.1109/TITS.2023.3285442).
- [19] W. Gao, Z.-P. Jiang, and K. Ozbay, "Data-driven adaptive optimal control of connected vehicles," *IEEE Trans. Intell. Transp. Syst.*, vol. 18, no. 5, pp. 1122–1133, May 2017.
- [20] M. Huang, Z.-P. Jiang, and K. Ozbay, "Learning-based adaptive optimal control for connected vehicles in mixed traffic: Robustness to driver reaction time," *IEEE Trans. Cybern.*, vol. 52, no. 6, pp. 5267–5277, Jun. 2022.
- [21] T. Liu, L. Cui, B. Pang, and Z.-P. Jiang, "Data-driven adaptive optimal control of mixed-traffic connected vehicles in a ring road," in *Proc. 60th IEEE Conf. Decis. Control (CDC)*, Dec. 2021, pp. 77–82.
- [22] J. Berberich, J. Köhler, M. A. Müller, and F. Allgöwer, "Data-driven model predictive control with stability and robustness guarantees," *IEEE Trans. Autom. Control*, vol. 66, no. 4, pp. 1702–1717, Apr. 2021.
- [23] J. Coulson, J. Lygeros, and F. Dörfler, "Distributionally robust chance constrained data-enabled predictive control," *IEEE Trans. Autom. Control*, vol. 67, no. 7, pp. 3289–3304, Jul. 2022.
- [24] J. Wang, Y. Zheng, K. Li, and Q. Xu, "DeeP-LCC: Data-enabled predictive leading cruise control in mixed traffic flow," *IEEE Trans. Control Syst. Technol.*, vol. 31, no. 6, pp. 2760–2776, Nov. 2023.
- [25] J. Wang et al., "Implementation and experimental validation of data-driven predictive control for dissipating stop-and-go waves in mixed traffic," *IEEE Internet Things J.*, early access, Aug. 8, 2023, doi: [10.1109/IOT.2023.3303039](https://doi.org/10.1109/IOT.2023.3303039).
- [26] J. Coulson, J. Lygeros, and F. Dörfler, "Data-enabled predictive control: In the shallows of the DeePC," in *Proc. 18th Eur. Control Conf. (ECC)*, Jun. 2019, pp. 307–312.
- [27] I. Markovsky and F. Dörfler, "Behavioral systems theory in data-driven analysis, signal processing, and control," *Annu. Rev. Control*, vol. 52, pp. 42–64, Jan. 2021.
- [28] J. C. Willems, P. Rapisarda, I. Markovsky, and B. L. M. De Moor, "A note on persistency of excitation," *Syst. Control Lett.*, vol. 54, no. 4, pp. 325–329, Apr. 2005.
- [29] L. Huang, J. Coulson, J. Lygeros, and F. Dörfler, "Decentralized data-enabled predictive control for power system oscillation damping," *IEEE Trans. Control Syst. Technol.*, vol. 30, no. 3, pp. 1065–1077, May 2022.
- [30] E. Eloksa, J. Coulson, P. N. Beuchat, J. Lygeros, and F. Dörfler, "Data-enabled predictive control for quadcopters," *Int. J. Robust Nonlinear Control*, vol. 31, no. 18, pp. 8916–8936, Dec. 2021.
- [31] J. Petit and S. E. Shladover, "Potential cyberattacks on automated vehicles," *IEEE Trans. Intell. Transp. Syst.*, vol. 16, no. 2, pp. 546–556, Apr. 2015.
- [32] M. Amoozadeh et al., "Security vulnerabilities of connected vehicle streams and their impact on cooperative driving," *IEEE Commun. Mag.*, vol. 53, no. 6, pp. 126–132, Jun. 2015.
- [33] X. Sun, F. R. Yu, and P. Zhang, "A survey on cyber-security of connected and autonomous vehicles (CAVs)," *IEEE Trans. Intell. Transp. Syst.*, vol. 23, no. 7, pp. 6240–6259, Jul. 2022.
- [34] F. Farivar, M. S. Haghghi, A. Jolfaei, and S. Wen, "On the security of networked control systems in smart vehicle and its adaptive cruise control," *IEEE Trans. Intell. Transp. Syst.*, vol. 22, no. 6, pp. 3824–3831, Jun. 2021.
- [35] R. A. Biroon, P. Pisu, and Z. Abdollahi, "Real-time false data injection attack detection in connected vehicle systems with PDE modeling," in *Proc. Amer. Control Conf. (ACC)*, Jul. 2020, pp. 3267–3272.
- [36] H. Gao, Z. Li, and Y. Wang, "Privacy-preserving collaborative estimation for networked vehicles with application to collaborative road profile estimation," *IEEE Trans. Intell. Transp. Syst.*, vol. 23, no. 10, pp. 17301–17311, Oct. 2022.
- [37] A. Jarouf, N. Meskin, S. Al-Kuwari, M. Shakerpour, and C. G. Cassandras, "Security analysis of merging control for connected and automated vehicles," in *Proc. IEEE Intell. Vehicles Symp. (IV)*, Jun. 2022, pp. 1739–1744.
- [38] M. Kamal, M. Tariq, G. Srivastava, and L. Malina, "Optimized security algorithms for intelligent and autonomous vehicular transportation systems," *IEEE Trans. Intell. Transp. Syst.*, vol. 24, no. 2, pp. 2038–2044, Feb. 2023.
- [39] T. Li, L. Lin, and S. Gong, "AutoMPC: Efficient multi-party computation for secure and privacy-preserving cooperative control of connected autonomous vehicles," in *Proc. SafeAI@ AAAI*, 2019.
- [40] S. G. Ezabadi, A. Jolfaei, L. Kulik, and R. Kotagiri, "Differentially private streaming to untrusted edge servers in intelligent transportation system," in *Proc. 18th IEEE Int. Conf. Trust, Secur. Privacy Comput. Commun./13th IEEE Int. Conf. Big Data Sci. Eng. (TrustCom/BigDataSE)*, Aug. 2019, pp. 781–786.
- [41] S. Ghane, A. Jolfaei, L. Kulik, K. Ramamohanarao, and D. Puthal, "Preserving privacy in the Internet of Connected Vehicles," *IEEE Trans. Intell. Transp. Syst.*, vol. 22, no. 8, pp. 5018–5027, Aug. 2021.
- [42] K. Zhang, K. Chen, Z. Li, and Y. Zheng, "Privacy-preserved data-enabled predictive control for connected and automated vehicles in mixed traffic," in *Proc. IEEE 25th Int. Conf. Intell. Transp. Syst. (ITSC)*, Oct. 2022, pp. 2648–2654.
- [43] A. A. H. Damen, P. M. J. Van den Hof, and A. K. Hajdasinski, "Approximate realization based upon an alternative to the Hankel matrix: The page matrix," *Syst. Control Lett.*, vol. 2, no. 4, pp. 202–208, Dec. 1982.

- [44] A. Sultangazin and P. Tabuada, "Symmetries and isomorphisms for privacy in control over the cloud," *IEEE Trans. Autom. Control*, vol. 66, no. 2, pp. 538–549, Feb. 2021.
- [45] K. Zhang, Z. Li, Y. Wang, and N. Li, "Privacy-preserved nonlinear cloud-based model predictive control via affine masking," 2021, *arXiv:2112.10625*.
- [46] J. Berberich, J. Köhler, M. A. Müller, and F. Allgöwer, "Linear tracking MPC for nonlinear systems—Part II: The data-driven case," *IEEE Trans. Autom. Control*, vol. 67, no. 9, pp. 4406–4421, Sep. 2022.
- [47] J. R. Salvador, D. R. Ramírez, T. Alamo, D. M. de la Peña, and G. García-Marin, "Data driven control: An offset free approach," *Tech. Rep.*, 2019, pp. 23–28. [Online]. Available: https://ieeexplore.ieee.org/abstract/document/8795956?casa_token=VMh2vCHyZiMAAAAA:3QzfTtV04CQ3PE5bzh-AApnf6szGeX_nyPcFbrQ71NkRjRPEGb9yFQJglmnk-2jxvxFLmX3g_
- [48] A. Machanavajjhala, D. Kifer, J. Gehrke, and M. Venkitasubramaniam, "L-diversity: Privacy beyond k-anonymity," *ACM Trans. Knowl. Discov. Data*, vol. 1, no. 1, pp. 3–14, 2007.
- [49] M. S. Darup, A. Redder, I. Shames, F. Farokhi, and D. Quevedo, "Towards encrypted MPC for linear constrained systems," *IEEE Control Syst. Lett.*, vol. 2, no. 2, pp. 195–200, Apr. 2018.
- [50] A. B. Alexandru, M. Morari, and G. J. Pappas, "Cloud-based MPC with encrypted data," in *Proc. IEEE Conf. Decis. Control (CDC)*, Dec. 2018, pp. 5014–5019.
- [51] DieselNet. (2013). *Emission Test Cycles ECE 15 + EUDC/NEDC*. [Online]. Available: https://dieselnet.com/standards/cycles/ece_eudc.php
- [52] D. P. Bowyer, R. Akçelik, and D. C. Biggs, *Guide to Fuel Consumption Analyses for Urban Traffic Management*. Melbourne, VIC, Australia: Australia Road Research Board, 1985.
- [53] K. Zhang, Y. Zheng, C. Shang, and Z. Li, "Dimension reduction for efficient data-enabled predictive control," *IEEE Control Syst. Lett.*, vol. 7, pp. 3277–3282, 2023.
- [54] J. Wang, Y. Lian, Y. Jiang, Q. Xu, K. Li, and C. N. Jones, "Distributed data-driven predictive control for cooperatively smoothing mixed traffic flow," *Transp. Res. C, Emerg. Technol.*, vol. 155, Oct. 2023, Art. no. 104274.
- [55] Next Generation Simulation (NGSIM) Vehicle Trajectories and Supporting Data, U.S. Department of Transportation Federal Highway Administration, Washington, DC, USA, 2016, doi: [10.21949/1504477](https://doi.org/10.21949/1504477).
- [56] H. J. van Waarde, C. De Persis, M. K. Camlibel, and P. Tesi, "Willems' fundamental lemma for state-space systems and its extension to multiple datasets," *IEEE Control Syst. Lett.*, vol. 4, no. 3, pp. 602–607, Jul. 2020.



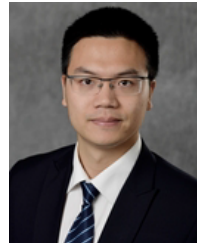
Kaixiang Zhang received the B.E. degree in automation from Xiamen University, Xiamen, China, in 2014, and the Ph.D. degree in control science and engineering from Zhejiang University, Hangzhou, China, in 2019.

From 2017 to 2018, he was a Visiting Doctoral Student with the National Institute for Research in Computer Science and Automation, Rennes, France. He is currently a Post-Doctoral Researcher with the Department of Mechanical Engineering, Michigan State University. His current research interests include visual servoing, robotics, and control theory and application.



Kaian Chen received the B.S. degree in electrical engineering from Nantong University, Nantong, China, in 2013, the M.S. degree in electrical and computation engineering from Ohio State University, Columbus, OH, USA, in 2017, and the Ph.D. degree in mechanical engineering from Michigan State University, East Lansing, MI, USA, in 2022.

His current research interests include nonlinear system identification, model predictive control, and autonomous vehicles.



Zhaojian Li (Senior Member, IEEE) received the M.S. and Ph.D. degrees in aerospace engineering (flight dynamics and control) from the University of Michigan, Ann Arbor, in 2013 and 2015, respectively. He was an Algorithm Engineer with General Motors from January 2016 to July 2017. He is currently a Red Cedar Distinguished Associate Professor with the Department of Mechanical Engineering, Michigan State University. His current research interests include learning-based control, nonlinear and complex systems, and robotics and automated vehicles. He is the author of more than 50 top journal articles and several patents. He was a recipient of the NSF CAREER Award. He is currently an Associate Editor of *IEEE TRANSACTIONS ON INTELLIGENT VEHICLES, Evolving Systems* journal, American Control Conference, and ASME Dynamics and Control Conference.



Jun Chen (Senior Member, IEEE) received the bachelor's degree in automation from Zhejiang University, Hangzhou, China, in 2009, and the Ph.D. degree in electrical engineering from Iowa State University, Ames, IA, USA, in 2014.

He is currently an Assistant Professor with the ECE Department, Oakland University. His current research interests include artificial intelligence and optimal control, with applications in intelligent vehicles and energy systems. He is a member of SAE. He was a recipient of the NSF CAREER Award,

the Best Paper Award from *IEEE TRANSACTIONS ON AUTOMATION SCIENCE AND ENGINEERING*, the Best Paper Award from IEEE International Conference on Electro Information Technology, the Faculty Recognition Award for Research from Oakland University, the Publication Achievement Award from Idaho National Laboratory, the Research Excellence Award from Iowa State University, and the Outstanding Student Award from Zhejiang University.



Yang Zheng (Member, IEEE) received the B.E. and M.S. degrees from Tsinghua University, Beijing, China, in 2013 and 2015, respectively, and the D.Phil. (Ph.D.) degree in engineering science from the University of Oxford, U.K., in 2019.

He was a Research Associate with Imperial College London and a Post-Doctoral Scholar in SEAS and CGBC with Harvard University. He is currently an Assistant Professor with the Department of Electrical and Computer Engineering, University of California at San Diego, CA, USA. His current research interests include learning, optimization, and control of network systems, and their applications to autonomous vehicles and traffic systems. He was a Finalist (coauthor) for the Best Student Paper Award at the 2019 European Control Conference (ECC). He was a recipient of the Best Student Paper Award at the 17th IEEE Conference on Intelligent Transportation Systems in 2014, the Best Paper Award at the 14th Intelligent Transportation Systems Asia-Pacific Forum in 2015, the 2019 European Ph.D. Award on Control for Complex and Heterogeneous Systems, the 2022 Best Paper Award in *IEEE TRANSACTIONS ON CONTROL OF NETWORK SYSTEMS*, and the Outstanding Survey Paper Award in *IEEE Intelligent Transportation Systems Magazine* from 2017 to 2020. He was also a recipient of the National Scholarship, the Outstanding Graduate at Tsinghua University, the Clarendon Scholarship at the University of Oxford, and the Chinese Government Award for Outstanding Self-financed Students Abroad.